AD-A111 826 IRT CORP SAN DIEGO CA F/G 4/1
INVERSE SCATTERING FOR ELECTRON DENSITY PROFILE DETERMINATION. --ETC(U)
SEP 81 W R STONE F19628-80-C-0187
UNCLASSIFIED IRT-8205-003-VOL-1 AFGL-TR-81-0282-VOL-1 NL

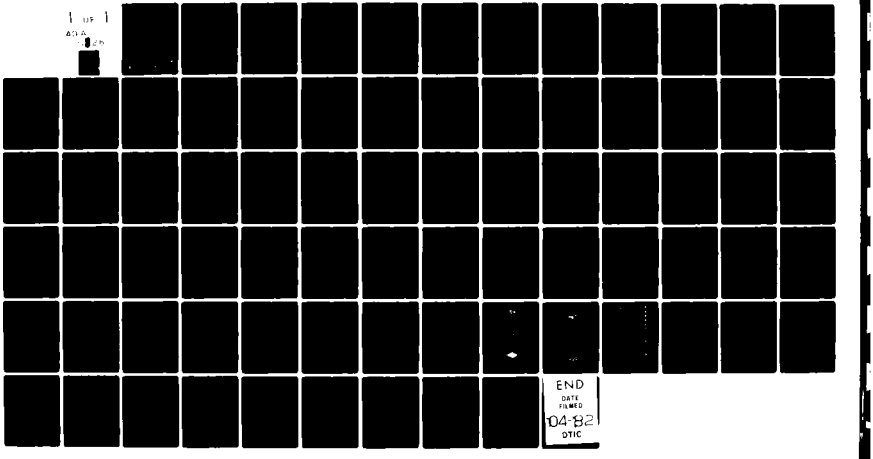

END
DATE FILMED
04-82
DTIC

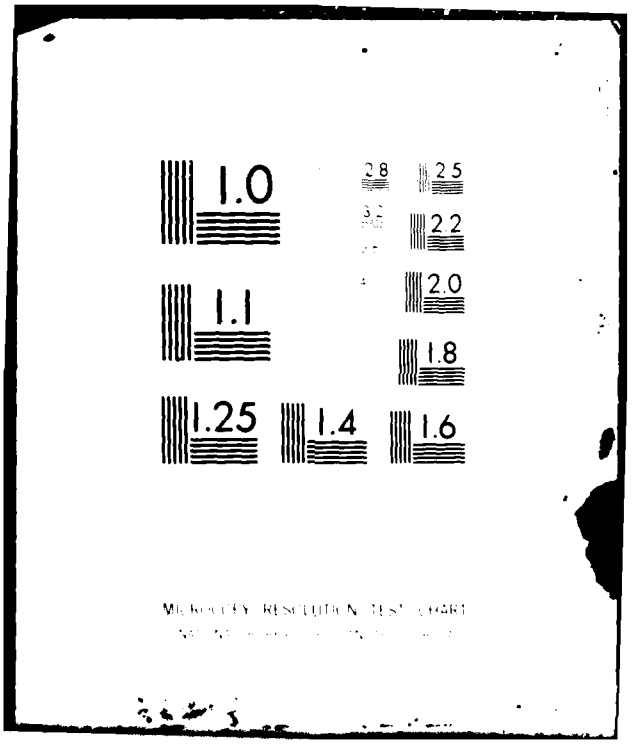
1.0
2.8
2.5
3.2
2.2
2.0
1.1
1.8
1.25
1.4
1.6

(9)

AFGL-TR-81-0282(I)

INVERSE SCATTERING FOR ELECTRON DENSITY PROFILE DETERMINATION
Volume I

W. Ross Stone

IRT Corporation
7650 Convoy Court
P. O. Box 80817
San Diego, California 92138

Final Report
August 28, 1980 to October 30, 1981

24 September 1981

Approved for public release; distribution unlimited

AIR FORCE GEOPHYSICS LABORATORY
AIR FORCE SYSTEM COMMAND
UNITED STATES AIR FORCE
HANSCOM AFB, MASSACHUSETTS 01731

UNCLASSIFIED

SECURITY CLASSIFICATION OF THIS PAGE (When Data Entered)

REPORT DOCUMENTATION PAGE		READ INSTRUCTIONS BEFORE COMPLETING FORM
1. REPORT NUMBER AFGL-TR-81-0282(I)	2 GOVT ACCESSION NO. AD-A111826	3. RECIPIENT'S CATALOG NUMBER
4. TITLE (and Subtitle) INVERSE SCATTERING FOR ELECTRON DENSITY PROFILE DETERMINATION Volume I		5. TYPE OF REPORT & PERIOD COVERED Final Report 8/28/80-10/30/81 6 PERFORMING ORG. REPORT NUMBER IRT 8205-003
7. AUTHOR(s) W. Ross Stone		8. CONTRACT OR GRANT NUMBER(s) F19628-80-C-0187
9. PERFORMING ORGANIZATION NAME AND ADDRESS IRT Corporation 7650 Convoy Court, P. O. Box 80817 San Diego, California 92138		10 PROGRAM ELEMENT, PROJECT, TASK AREA & WORK UNIT NUMBERS 61102F 2310G6AB
11. CONTROLLING OFFICE NAME AND ADDRESS Air Force Geophysics Laboratory Hanscom AFB, Massachusetts 01731 Monitor/Milton M. Klein/PHY		12. REPORT DATE 24 September 1981 13 NUMBER OF PAGES 76
14. MONITORING AGENCY NAME & ADDRESS(if different from Controlling Office)		15. SECURITY CLASS. (of this report) Unclassified 15a. DECLASSIFICATION/DOWNGRADING SCHEDULE
16. DISTRIBUTION STATEMENT (of this Report) Approved for public release; distribution unlimited		
17. DISTRIBUTION STATEMENT (of the abstract entered in Block 20, if different from Report)		
18. SUPPLEMENTARY NOTES		
19. KEY WORDS (Continue on reverse side if necessary and identify by block number) Inverse scattering Ionosphere Electron density profile Inverse source problem Nonradiating sources		
20. ABSTRACT (Continue on reverse side if necessary and identify by block number) The application of Exact Inverse Scattering Theory to the determination of the spatial distribution of ionospheric electron density is investigated. Vector field measurements and the effects of the earth's magnetic field are included. The uniqueness of the solution is proven for these cases. An exact analytic, closed-form solution for the source term in the inverse scattering problem is obtained. Practical and numerical aspects of using the techniques developed are examined.		

DD FORM 1 JAN 73 1473 EDITION OF 1 NOV 65 IS OBSOLETE

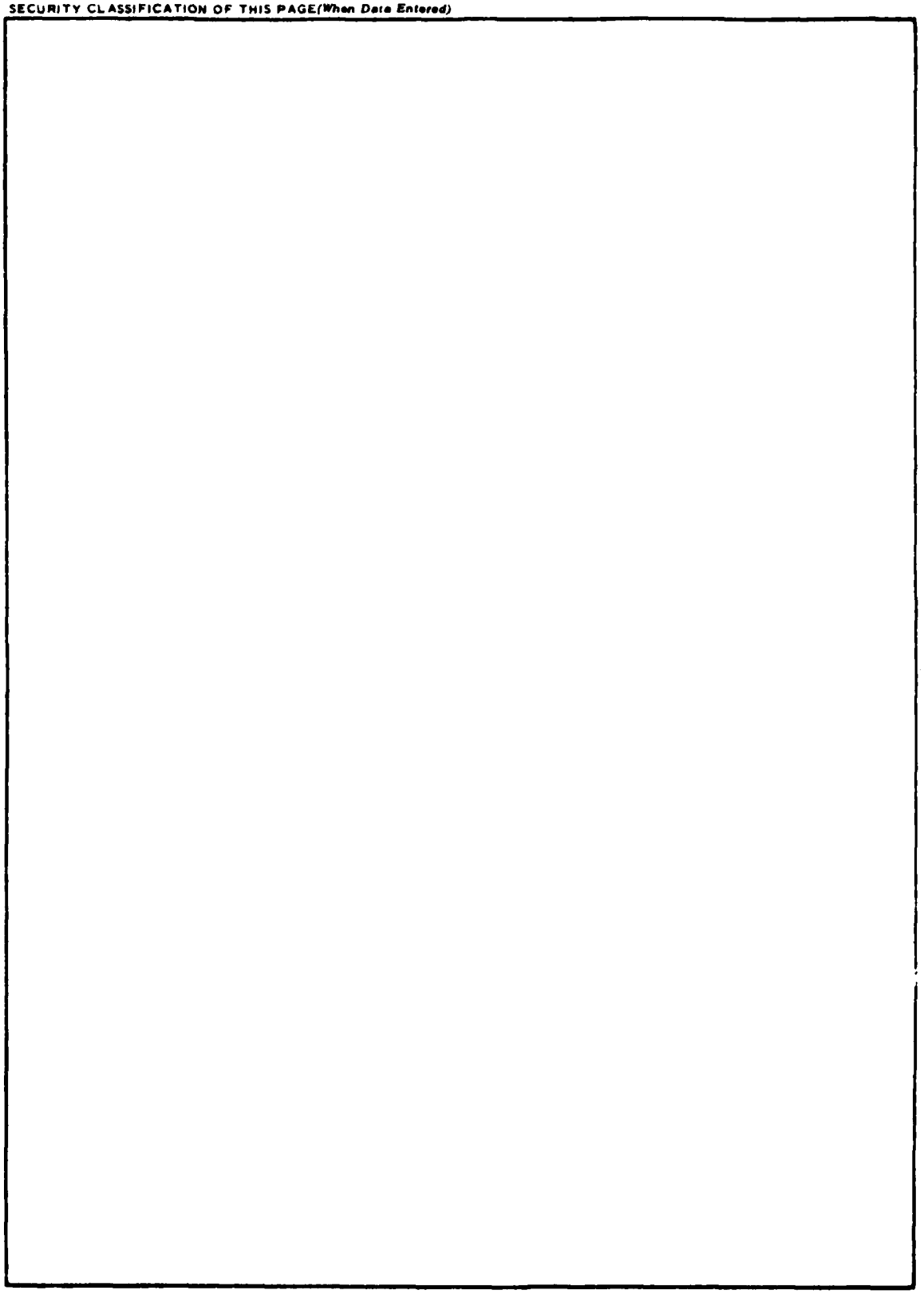

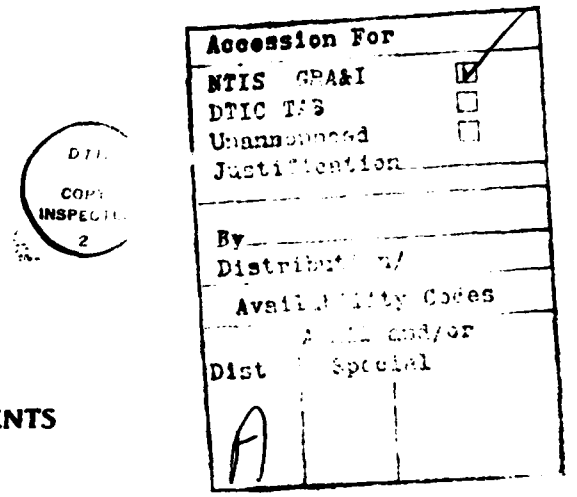

TABLE OF CONTENTS

TABLE OF CONTENTS (continued)

1. INTRODUCTION

This document is the final report on Contract F19628-80-C-0187. The purpose of the research reported herein is to study the feasibility of determining ionospheric electron density profiles from measurements of the scattering of electromagnetic waves entering the ionosphere from outside the earth's atmosphere. This is an inverse scattering problem, and the approach used is to develop a practical procedure based on inverse scattering theory.

A detailed literature survey on the application of existing approaches to the determination of the electron density distribution in the ionosphere led to the conclusion that the best approach was to apply the Exact Inverse Scattering Theory, developed by N. N. Bojarski, to the problem. This literature survey is contained in Volume II of this report. Comments on the results of the survey are included in this section. This section also defines the specific problem being addressed in more detail, and examines the relationships among the desired quantity, measurable quantities, and the physical parameters useful from a theoretical standpoint. Section 2 reviews the derivation of the Exact Theory. In addition, the theory is cast into a form including full vector electromagnetic fields and the effects of a uniform magnetic field. Section 3 examines the uniqueness of the solution obtained using the Exact Theory, and extends the author's earlier uniqueness proof for the scalar case to the full anisotropic medium, vector electromagnetic case. Prior to 1980, the uniqueness of the solution to the inverse scattering problem was complicated by the question of nonradiating sources. In 1980, this author presented a proof that while nonradiating sources are mathematically permissible within the context of inverse scattering theory, the fields they produce are physically inconsistent with the wave equation governing the problem. During the course of this research, two additional independent verifications that nonradiating sources are physically unrealizable became available, as reported in Section 3.

Perhaps the most important and exciting results to come out of this research are presented in Section 4. Late in 1980, Bojarski obtained an exact closed-form, analytic solution for the total fields (including fields in the source region) in the inverse scattering problem. This solution has the same importance for the inverse problem as the Kirchhoff and Stratton-Chu equations have for the direct scattering problem.

Subsequently, the author was able to obtain two results. First, the solution obtained by Bojarski was cast into a form involving only known quantities and Fourier transforms of the measured data. This makes the new solution for the fields practical for application to problems such as the electron density profiling problem. It also renders the computations associated with evaluating the new solution numerically as efficient as the fast Fourier transform, both in speed and storage. Second, and even more important, the author was able to obtain an exact, closed-form, analytic solution for the source term in the inverse scattering problem. This also is expressed in terms of only known quantities and Fourier transforms of the measured data. Perhaps the most pleasing aspect of these results is the tremendous amount of new insight into the basic physics of inverse scattering (and, indeed, into fundamental field theory) which they provide. As should be the case in a true research effort, these results were not anticipated before the research was begun.

It is worth putting these new results into perspective with the previous status of the Exact Theory, on which they are based. Until now, it was necessary to solve an integral equation numerically to obtain the sources, and thence the refractive index and the electron density profile. Although this equation should have an efficient, numerically stable method of solution it did not have the advantages of an analytic solution. The new results provide analytic solutions for both the fields and the sources in the inverse scattering problem.

Section 5 summarizes the results of analytical and numerical simulation work performed to demonstrate how the electron density distribution can be determined using inverse scattering. It was originally desired to simulate scattering by an ionosphere that is inhomogeneous in two or three dimensions, and apply the inverse scattering techniques to obtain a reconstruction of the simulated electron density distribution. Substantial problems were encountered in carrying out the simulations, because of difficulties in modeling the direct scattering problem. These results are necessary because they constitute the simulated data used as input for the inverse scattering calculations. However, it was possible to demonstrate the stability of the numerical solution for the inverse scattering approach. Several methods of computing the required direct scattering data were tried, and a number of approximations heretofore overlooked in the literature on scattering by inhomogeneous media in general and on scattering by the ionosphere in particular were identified. These results have important implications for other modeling studies. A method capable of providing the required direct scattering data was developed, and preliminary tests indicate that it

will provide the needed data for the desired two- and three-dimensional simulations in future work. Finally, as means of demonstrating what should be achievable in applying the Exact Theory to two- and three-dimensional inhomogeneities, a related, one-dimensional, time domain simulation was carried out. The results demonstrate the capability to reconstruct realistic one-dimensional ionospheric profiles, in the presence of realistic experimental noise. Furthermore, the capability to determine the profile above the maximum in electron density using only bottom-side vertical incidence sounder data was demonstrated. To the author's knowledge this is the first time such a capability has been demonstrated even in simulation in the presence of realistic amounts of measurement noise. The technique should be directly applicable to the analysis of data from a large class of existing ionospheric sounders.

Section 6 discusses the practical aspects of applying the theory and results of the previous sections to the experimental determination of the electron density distribution. In particular, it is shown that while the effects of the earth's magnetic field can be included in the analysis, it is not necessary to do so. Proper choice of the frequency of the electromagnetic wave used to probe the ionosphere eliminates this complication and simplifies the required measurements.

Section 7 presents the conclusions drawn from this research and provides recommendations for further work.

This paper has aspects of both a report of new results and a review. This was done in a conscious effort to make the result self-contained. Readers familiar with the author's earlier review papers on exact inverse scattering theory should feel free to skip those sections which appear familiar.

1.1 PROBLEM DEFINITION AND THE CONCEPT OF INVERSE SCATTERING

The purpose of this research is to develop a technique for determining the three-dimensional spatial distribution of electron density in the ionosphere. This information is to be determined from measurements of the scattering of electromagnetic waves entering the ionosphere from outside the earth's atmosphere. It is assumed that these measurements are to be ground based, and that the source of the electromagnetic waves is known. The availability of a satellite beacon as a source can be assumed. By definition, this is an inverse scattering problem.

As discussed below, the distinction between a direct scattering and an inverse scattering problem is based upon what is known and what is sought in the problem. In a direct scattering problem, the source of the fields, the geometry, and the medium properties involved are all known; the scattered fields are sought. In an inverse

scattering problem, the scattered fields are measured and thus known. What is sought is a description of the sources in the problem. In the problem under consideration, the ionosphere is probed using an electromagnetic field, and the scattered field (or the sum of the incident and scattered fields) is measured, and thus known. What is sought is the electron density as a function of three spatial dimensions. Because the probing wave interacts with the density variations by inducing currents in the medium (which may be viewed as the sources of the scattered field), the desired information about the electron density profile is contained in this induced source term. Thus, in this problem, the fields are measured and the (induced) source term is sought; the determination of the electron density profile is an inverse scattering problem. These concepts are made clearer in the mathematical presentation below.

Inverse scattering as a field has existed for about 50 years. It originated in the quantum mechanists' need to determine the scattering potential of an atomic system from scattering data. Because of this basis, inverse problems have been thought to have inherently ill-posed and nonunique solutions with little or no practical application. This view has been due largely to the development of inverse scattering theory from a discipline in which coherent field measurements are impossible, and in which it was the *scattering potential* that was sought rather than the source term in the wave equation. Recently, N. N. Bojarski has developed an Exact Inverse Scattering Theory that overcomes these limitations. It is this theory that forms the basis for the research reported in this paper. It is applicable to quite general electromagnetic and acoustic problems. As presented below, its solution has been proven unique, well-posed, and possessing properties which make it eminantly applicable to practical applications.

The ionosphere is a low-temperature (but not "cold") plasma existing in the presence of the earth's magnetic field and in the presence of a complex, temporally and spatially varying background of neutral and ionic components. Literal determination of the three-dimensional spatial distribution of electron density could imply knowledge of the position of each electron at an instant of time. This is neither possible or desired. The purpose for which a measure of the electron density distribution is wanted is to understand and predict ionospheric effects on electromagnetic propagation (e.g., for communications) and to understand ionospheric morphology. These effects depend on electron density distributions over a wide range of scale sizes. There is strong evidence for this scale size range to extend from less than 1 m to an appreciable fraction of the radius of the earth (Ref 1). For almost all purposes related to structural and propagation studies, the distances over which variations in electron density are of importance are at least several meters, and often many orders of magnitude larger than

this. This means that the spatial resolution with which the electron density needs to be determined is on a macroscopic scale with respect to molecular and ionic constituent interactions with the probing and scattered fields. Limitation to such macroscopic scales is also justified based on the spatial resolution usually available for field measurements.

The ability to view the electromagnetic scattering process--and thus the inverse scattering problem--on a macroscopic scale is of considerable importance. As discussed in the next subsection, the inverse scattering theory as it is applied to this problem is based on the ability to express the fundamental physics of the problem in terms of a linear wave equation and a constitutive relationship. This formulation is quite accurate for the ionosphere on a macroscopic scale. However, on a microscopic scale radiation transport theory must be employed, and the equations are usually nonlinear and much more complex. This is not the problem under consideration here.

A comment on terminology is in order. The problem addressed by this research has been termed the determination of the electron density "profile." Historically, among the first experimental determinations of the spatial variation in electron density in the ionosphere were vertical incidence sounder measurements of the apparent variation in density with height: The vertical electron density profile. Use of the term "profile" strictly implies a one-dimensional variation. It is well known that variations in ionospheric electron density in all three dimensions are of fundamental importance in many problems, and the research reported in this paper is directed towards obtaining three-dimensional information. However, it is sometimes easier to use the term "profile" as if it includes two- and three-dimensional variations instead of always explicitly stating that three-dimensional variations are meant.

1.2 MEASURABLE QUANTITIES, CALCULABLE QUANTITIES, AND THE ELECTRON DENSITY

On a macroscopic scale, electromagnetic waves interact with the permeability and permittivity variations of the medium. The measured quantity in this problem is the electromagnetic field, and the desired quantity is the electron density distribution. In order to go from the measured fields to the desired electron density it is necessary to have a set of equations relating these quantities: This is provided by the inverse scattering theory presented in the following sections. It is important to distinguish between those equations that represent rigorous electromagnetic theory and those that assume a physical model for the ionosphere.

The Exact Theory provides equations which can be solved for the total field, $\phi(\underline{x},\omega)$, and the source term, $\rho(\underline{x},\omega)$, in the wave equation governing propagation in the medium. Given that Maxwell's equations and the wave equation derived from them apply to the ionosphere (which is certainly a good assumption for macroscopic interactions), these solutions are rigorous and do not involve models. The source term contains the effects of inhomogeneities in the medium in the form of induced sources, due to the interaction between the probing wave and the medium. In order to relate the sources and fields to the macroscopic permeability and permittivity it is necessary to have a constitutive relation. The form of this relation chosen in the derivation below is (for the scalar case)

$$\rho(\underline{x},\omega) = k^2 \left[n^2(\underline{x},\omega)-1 \right] \phi(\underline{x},\omega) \tag{1}$$

where $k = 2\pi/\lambda$, λ is the free space wavelength and n is the complex refractive index. It is convenient to work in terms of the complex refractive index rather than the (equivalent) permeability and permittivity. This form of the constitutive relation can be derived directly from Maxwell's equations for a plasma with a uniform magnetic field (e.g., Ref 2, pp. 63-67). No other assumptions about the medium are involved in arriving at a constitutive relation of the form of Equation 1. However, additional modeling assumptions are necessary to relate the refractive index to the electron density and to the other physical properties of the medium. It will be shown in Sect 6 that the Appleton-Hartree equation relating the refractive index to the electron density and other medium properties is a very good model for use with the methods of determining the electron density distribution discussed in this paper. Indeed, use of this model results in a particularly simple relationship among ρ, ϕ, n, and the electron density. In fact, under certain conditions that are usually possible to ensure in an experiment, it can be shown that the intermediate steps of solving for ρ and n are unnecessary. It is possible to compute a quantity directly from the measured fields that is proportional to the electron density. This is discussed in Section 6.

It should also be noted that the inverse scattering theory results derived in the following sections are applicable whenever propagation in the ionosphere can be expressed in terms of the wave equation employed below. Different applications to the ionosphere may require different constitutive relations and/or different relations between n and the medium properties. However, the method of solving for the source term is independent of the constitutive relationship.

1.3 RESULTS OF LITERATURE SURVEY

An extensive, computer-aided literature survey was carried out as part of this research. An annotated bibliography of references related to inverse scattering techniques that could be applied to the problem of determining the three-dimensional variation of electron density in the ionosphere is included in Volume II. Based on this survey, it was concluded that the Exact Inverse Scattering Theory of N. N. Bojarski, as applied by the author and other workers in the field, combined with the Holographic Radio Camera technique developed by the author (Refs 3-5), is best suited for addressing the problem considered in this research.

The primary problem with other inverse scattering techniques is that they suffer one or more of three limitations: They are applicable only to one-dimensional problems; they are ill-posed in the presence of measurement noise; or they involve approximations which may be acceptable for problems involving some types of scatterers (e.g., the physical optics and far-field approximations often used for scattering by conducting bodies) but which are not applicable to the ionosphere. Indeed, it can be argued with mathematical rigor that since the Exact Theory is both exact and has a unique solution (see Section 3), it is the only truly correct approach.

As an example of the typical situation found in doing the survey, one other candidate technique which has been applied analytically to determine the electron density profile is the work of Jordan and Ahn (see, for example, Ref. 6 and references therein). Their approach, in work which has continued over the last decade, is to use Kay's and Kay and Moses' extension of the Gelfand-Levitan solution for one-dimensional inverse problems. In particular, they are able to solve problems in which the profile can be modeled using an analytic function with a small number of poles (e.g., one to three). Based on the information available in the literature, this approach suffers from three very serious limitations for application to the problem addressed by this paper. First, the approach has not been demonstrated to be applicable to problems in two and three dimensions. Second, the behavior of the approach in the presence of measurement noise has not been investigated. This is of considerable concern, because what the approach is based upon--the Gelfand-Levitan solution--is usually considered to be unstable with respect to such noise. Third, in a recent paper by Reilly and Jordan (Ref 7), it was shown that the number of poles required to approach a reasonable approximation of even a one-dimensional ionospheric profile is of the order of 40,000 or more. The authors readily admitted that the technique was probably not applicable for such problems.

2. THE EXACT INVERSE SCATTERING THEORY

2.1 THE INTEGRAL EQUATION FOR INVERSE SCATTERING

This subsection presents a derivation of N. N. Bojarski's (Refs 8-11) "Exact Inverse Scattering Theory." The theory is derived in the form leading to an integral equation which can be solved numerically in a stable and efficient manner. Section 4 presents derivations which parallel that of this section, but which result in exact, closed-form analytic solutions for the total field and the source term. This order of presentation has been chosen because it has proven to be the simplest for newcomers to the field of inverse scattering to understand. It is important to note that although consideration of the integral equation is the simplest means of introducing the Exact Theory, the analytic solutions of Section 4 are by far the most significant results presented in this paper.

Although scalar notation is used in the derivation of this subsection and elsewhere in this paper, unless otherwise noted <u>all</u> of the results presented have been shown <u>rigorously</u> to apply to the full vector electromagnetic equations for an anisotropic medium. Specifically, they apply to the ionosphere in the presence of a uniform magnetic field (see also the discussions in Sections 1.2 and Section 6).

Consider a source $\rho(\underline{x})$ in a domain D bounded by a surface S. Then the time harmonic field, $\phi(\underline{x})$, due to $\rho(\underline{x})$ is the solution to the inhomogeneous wave equation

$$\nabla^2\phi(\underline{x}) + k^2\phi(\underline{x}) = -\rho(\underline{x}), \quad \underline{x} \in D \tag{2}$$

where $k = 2\pi/\lambda$.

A direct scattering problem is one in which $\rho(\underline{x})$ is known or specified, and a solution for $\phi(\underline{x})$ is sought. The inverse scattering problem is one in which $\phi(\underline{x})$ is known, and $\rho(\underline{x})$ is sought. For the inverse <u>source</u> problem, $\phi(\underline{x})$ is measured over some surface, and the object is to determine $\rho(\underline{x})$. In general, $\rho(\underline{x}) = \rho_m(\underline{x}) + \rho_s(\underline{x})$, where ρ_m is due to interaction with the medium, and ρ_s is due to actual sources. If $n(\underline{x})$ is the complex refractive index of the medium, then

$$\rho_m(\underline{x}) = k^2 \left[n^2(\underline{x}) - 1 \right] \phi(\underline{x}) \tag{3}$$

In most remote probing problems, $\rho_s(\underline{x})$ is known, and $\rho_m(\underline{x})$ is sought to yield n(x). This is termed the inverse medium problem. If $\phi(\underline{x})$ is specified (as the desired field) and $\rho(\underline{x})$ or $n(\underline{x})$ is sought so as to produce that $\phi(\underline{x})$, the problem is termed an inverse synthesis problem. This paper deals with an inverse medium problem.

Let the following field quantity, $\phi_H(\underline{x})$, be defined:

$$\phi_H(\underline{x}) = \oint \left[g^*(\underline{x}-\underline{x}')\nabla\phi(\underline{x}') - \phi(\underline{x}')\nabla g^*(\underline{x}-\underline{x}') \right] d\underline{S}' \tag{4}$$

where $g(\underline{x})$ is the free space Green's function and the asterisk denotes complex conjugation. g satisfies Equation 2 with $\rho(\underline{x}) = \delta(\underline{x})$. ϕ_H is in the form of the Kirchhoff integral with g complex conjugated. Note that if the Kirchhoff integral is applied to the field $\phi(\underline{x})$ on S and evaluated at any point $\underline{x}$ inside D, it is identically zero: The Kirchhoff integral is nonzero only for points outside D. Conversely, $\phi_H(\underline{x})$ is nonzero only for points inside D. Points outside of D are associated with the direct scattering problem; points inside D are of interest for the inverse scattering problem. This topological difference is the reason why direct scattering solutions are mathematically ill-posed when applied to the inverse scattering problem.

It should also be noted that ϕ_H is the mathematical expression for the reconstruction obtained from a hologram (ϕ in Equation 4) recorded on S. The relationship between holography and inverse scattering, along with an analysis of the consequences for remote probing and coherent imaging applications, has been presented by Stone (Reference 3; see Section 6). ϕ_H is, in general, known for inverse problems, since ϕ is known over S. ϕ is measured over S for the inverse source and medium problems, or specified over S for the inverse synthesis problem.

Applying Gauss' theorem to Equation 4 converts the surface integral into a volume integral:

$$\phi_H = \int dV \left(g^* \nabla^2 \phi - \phi \nabla^2 g^* \right) \tag{5}$$

From Equation 2,

$$\nabla^2\phi = -k^2\phi - \rho \tag{6}$$

and, by complex conjugation of Equation 2 for g,

$$\nabla^2 g^* = -k^2 g^* - \delta \tag{7}$$

Substitution of Equations 6 and 7 into Equation 5 gives

$$\phi_H = \int dV \left[g^*(-k^2\phi - \rho) - \phi(-k^2 g^* - \delta) \right]$$

$$= \int dV(\phi\delta - g^*\rho) \tag{8}$$

and, carrying out the integration over the delta function,

$$\phi_H = \phi - \int dV\, g^*\rho \tag{9}$$

Direct scattering theory gives the result that

$$\phi = \int dV\, g\, \rho + \oint dS(g\nabla\phi - \phi\nabla g)$$

$$= \int dV\, g\, \rho + \phi_i \tag{10}$$

In Equation 10, the first integral is just the superposition integral over the sources. The second term is the Kirchoff integral, and is associated with the incident field, ϕ_i. For the inverse scattering problem, ϕ_i can be assumed to be known without loss of generality (e.g., it is the known probing field for the inverse medium case, or the specified incident field in the inverse synthesis case).

Equations 9 and 10 are two independent simultaneous equations in two unknowns, ϕ and ρ. Substitution of Equation 10 into Equation 9 yields

$$\phi_H = \int dV\, g\, \rho - \int dV\, g^*\, \rho + \phi_i$$

$$= \int dV\, (g-g^*)\, \rho + \phi_i \qquad (11)$$

or

$$\phi_H(\underline{x}) = 2i \int dV'\, \mathrm{Im} g(\underline{x}-\underline{x}')\, \rho(\underline{x}') + \phi_i(\underline{x}) \qquad (12)$$

where Im denotes the imaginary part. Equation 12 is the basic equation of the Exact Inverse Scattering Theory. It is an integral, convolution equation for the single unknown, $\rho(\underline{x})$. It can be solved by standard deconvolution techniques. Quite recently, Stone has presented a closed-form solution to Equation 12, based on a closed-form solution by Bojarski for the total field, ϕ, in Equation 9 (see Section 4).

2.2 DETERMINATION OF THE IONOSPHERIC REFRACTIVE INDEX

Based on the above theory, the inverse medium problem can be solved by the following steps:

A. Compute $\phi_H(\underline{x})$, using the measured field values in Equation 4 (note that the surface of integration, S, is the measurement surface).

B. Solve Equation 12 for $\rho(\underline{x})$, using $\phi_H(\underline{x})$ from A and the known incident field, $\phi_i(\underline{x})$.

C. Compute the total field, $\phi(\underline{x})$, from the direct scattering result, Equation 10, using $\rho(\underline{x})$ from B.

D. Solve Equation 3 for the desired complex refractive index, $n(\underline{x})$, using $\rho(\underline{x})$ from B and $\phi(\underline{x})$ from C.

Note that for the inverse source problem, only steps A and B are required. However, for the inverse medium problem it is necessary to carry out steps C and D in addition. The solution to the direct scattering problem (step C) is a necessary step in solving the inverse medium problem. It is important to emphasize that the computations involved in steps A through C are all convolution integrals: They can be carried out using fast Fourier transform techniques. As a result, computation time and storage requirements are proportional to $N \log_2 N$, where N is the number of data points. Step D is an algebraic operation.

The closed-form, analytic solutions of Section 4 permit a closed-form, analytic solution to the inverse medium problem.

2.3 DETERMINATION OF THE IONOSPHERIC ELECTRON DENSITY

When, for example, the above four steps are applied to fields from a satellite-borne beacon which have propagated through the ionosphere and are measured on the surface of the earth, the three-dimensional complex refractive index of the ionosphere is obtained. As discussed in Section 1.2, it is necessary to have a model relating the refractive index to the electron density in order to obtain the electron density. As discussed in Section 6, the Appleton-Hartree formula (Reference 3, Section 2.3.2) is an excellent approximation under conditions that can usually be readily achieved in ionospheric measurement:

$$n^2 = 1 - X \Big/ \left\{ 1-iZ- \left[Y_T^2/2(1-X-iZ) \right] \pm \left[\left(Y_T^4/4(1-X-iZ)^2 \right) + Y_L^2 \right]^{1/2} \right\} \tag{13}$$

where, in the standard notation,

$$\begin{aligned} X &= Ne^2/\epsilon_o m\omega^2 \\ Y_L &= eB_L/m\omega \\ Y_T &= eB_T/m\omega \\ Z &= \nu/\omega \end{aligned} \tag{14}$$

with N being the (sought-after) electron number density, e is the charge and m is the mass of the electron, ϵ_o is the permittivity of free space, $\omega = 2\pi f$ is the angular frequency of the probing wave, ν is the collision frequency, and B is the magnetic field strength. The subscripts L and T denote the portion of the magnetic field longitudinal and transverse to the direction of the normal to the propagating wave. In the absence of the magnetic field ($Y_T = Y_L = 0$) and of collisions, the refractive index is purely real and given by

$$n^2 = 1 - X = 1 - K N/f^2 \tag{15}$$

where $K = e^2/4\pi^2\epsilon_o m = 80.5\ m^3Hz^2$ when N is in meters^{-3} and f is in Hertz. As discussed in Section 6, at high enough frequencies Equation 15 becomes an excellent approximation. In such cases, the scalar field treatment used above is adequate, and both the measurements and computations are simplified. To obtain the three-dimensional electron density distribution in this case, $n(\underline{x})$ from step D of Section 2.2 is substituted into Equation 15, which is solved for $N(\underline{x})$.

At lower frequencies the anisotropy of the ionosphere produced by the earth's magnetic field becomes important. Mathematically, this affects two aspects of applying the Exact Theory. First, the above derivation and, in particular, Equations 10 and 12, must be extended to include the full vector electromagnetic fields. The need for this can be seen immediately from the form of Equation 13: The refractive index is different for the components of the wave propagating transverse or longitudinal to the earth's magnetic field (indeed, such a difference is one definition of an anisotropic medium). Second, there are two unknown quantities on the right-hand side of Equation 13: N, and ν. In order to solve for both (or for either when the other is unknown) of these quantities, two linearly independent equations for n must be available. These are obtained by measuring the longitudinal and transverse field components, carrying out the solution to the vector equivalents of Equations 10 and 11 and steps A through D to obtain $n(\underline{x})$ for the longitudinal and transverse directions, and then solving these two equations simultaneously for $N(\underline{x})$ and $\nu(\underline{x})$. If the frequency of the probing wave is high enough that collisional effects are negligible (but not so high that the magnetic field effects can be neglected), then the two equations are solved in a least-squares sense (in the presence of measurement noise) to obtain $N(\underline{x})$.

It is important to note that in all of the derivations of this section, and in all of the material presented in this paper except for the time domain example discussed in Section 5, frequency is a parameter. This means that measurements and determination of $n(\underline{x},\omega)$, and thus of $N(\underline{x})$ (which, of course, is <u>independent</u> of frequency), can be carried out using a single frequency. If a band of frequencies is available, then this additional information can be used to discriminate against noise in the solution and, equivalently, to improve the spatial resolution of the determination of $N(\underline{x})$.

2.4 EXACT INVERSE SCATTERING THEORY FOR VECTOR FIELDS

To derive the vector analogue of Equations 10 and 12, a mixed vector field quantity ϕ_H is defined:

$$\underline{\phi}_H \equiv \oint dS \left[\underline{\nabla} g^* \times (\underline{a} \times \underline{H}) - \underline{\nabla} g^* (\underline{a} \cdot \underline{H}) + i\omega\epsilon_o g^* (\underline{a} \times \underline{E}) \right] \tag{16}$$

where $\underline{a} \times \underline{H}$ and $\underline{a} \cdot \underline{H}$ are the tangential and normal components of the magnetic field, respectively, over the measurement surface S, and $\underline{a} \times \underline{E}$ is the tangential component of the electric field over S. $\underline{a}$ is the unit normal vector. g^* is the complex conjugate of the free space Green's function. If the vector form of Green's first theorem is applied to Equation 16, and the same steps as were carried out in going from Equation 4 to Equation 12 are followed, the result is (Ref 9)

$$\underline{\phi}_H(\underline{x}) = 2i \int dV' \, \mathrm{Im} \underline{\nabla} g(\underline{x} - \underline{x}') \times \underline{J}(\underline{x}') \tag{17}$$

This equation should be compared with Equation 12.

The vector analogues of the direct scattering Equation 10 are the well-known Shatton-Chu equations for the $\underline{E}$ and $\underline{H}$ fields in terms of $\underline{J}$ (Reference 12, Section 8.14).

Use of Equations 16 and 17 according to the four-step solution process described in Section 2.2 requires a constitutive relation, analogous to Equation 3. The utility of the relation chosen for the vector case depends, to some extent, on the model that will be used to relate the medium properties in the constitutive relation to the desired electron density. As an illustration that is often a very good model for the ionosphere, the magneto-ionic theory (which led to the Appleton-Hartree equation for the refractive index used above) can be used. The vector magneto-ionic equations can be derived from either of two viewpoints: Considering the source of the fields to be conduction currents (c.f. Reference 12, Chapter 2), or considering the source to be displacement/polarization currents (c.f. Reference 13, Chapter 5). Equation 17 is written using $\underline{J}$, which implies the former approach. In order to most easily demonstrate the connection to the refractive index and electron density formulae used above, it is more convenient to write $\underline{J}$ in terms of the displacement current. In Cartesian coordinates, with z the direction of propagation and the earth's magnetic field in the x-z plane, the constitutive relation is thus (c.f. Reference 13, Equations 5.31-5.32 ff)

$$\begin{aligned} J_x &= i\omega\epsilon_o n^2 E_x \\ J_y &= i\omega\epsilon_o n^2 E_y \\ J_z &= 0 \end{aligned} \tag{18}$$

Although written as a scalar in Equation 18, the refractive index along the x and y directions does, in fact, differ, as discussed in Section 2.3. This can be seen from the form of the equation for n, Equation 13. The value of n depends on the values of Y_T and Y_L, which in turn depend on the orientation of E_x and E_y with respect to the magnetic field. To properly derive the form of Equation 18 that explicitly contains the transverse ($Y_L = 0$ in Equation 13) and longitudinal ($Y_T = 0$) values of n (i.e., n_L and n_T), it is necessary to introduce the concept of a polarization matrix for the fields. Expressions for E_x and E_y in terms of X, Y_L, Y_T, Z, and the transverse and longitudinal components of E are obtained by writing E_x and E_y in terms of their transverse and longitudinal components. Rather than repeating this extremely involved and, as will be shown below, unnecessary derivation here, the reader is referred to Reference 14, Sections 5.3-5.6 ff. When substituted into Equation 18, the result is two simultaneous equations. J_x and J_y are known from the solution to Equation 17, and the transverse and longitudinal components of $\underline{E}$ are known from the Shatton-Chu equations. The unknowns are X and Z, or the electron density distribution and the collision frequency. These two simultaneous equations are solved for these two unknowns.

While the above rather involved explanation is correct, it is also unnecessary in practice. It turns out that with proper choice of a coordinate system the scalar mathematical treatment of the previous sections can be employed. An orthogonal curvilinear set of coordinates is defined by the direction of the earth's magnetic field (which follows a curved path between the source of the probing field and the measurement region), and longitudinal (L) and transverse (T) coordinates everywhere orthogonal to each other and to the magnetic field. Then longitudinal and transverse field components can be measured on the surface of the earth, and they will each satisfy equations of the form of Equations 10 and 12. They will also satisfy the constitutive relation Equation 3, with n given by n_L ($Y_T = 0$ in Equation 13) for the longitudinal field and n given by n_T ($Y_L = 0$ in Equation 13) for the transverse component. This yields directly the two simultaneous equations for N and ν.

Finally, it should again be noted that proper choice of the probing wave frequency yields a real refractive index with N as the only unknown, and a scalar field propagation problem. This eliminates the requirement for measuring and processing vector fields. This is discussed in more detail in Section 6.

3. UNIQUENESS

If the solution for the source term can be shown to be unique, then the solution for the electron density (and, where applicable, the collision frequency) is unique in both the scalar and vector cases. This statement, of course, depends on the form of the constitutive relation and the model chosen for the ionosphere. Its truth for the magneto-ionic model can easily be seen from the discussions in Sections 2.3 and 2.4, and the algebraic form of the equations involved. The rigorous proof of the uniqueness of the solution for the source term is presented separately below for the scalar and vector equations. In both cases, it will be shown that the solution is unique if the source has compact support (i.e., is identically zero everywhere outside some finite domain), has finite energy, and does not contain any nonradiating components. A nonradiating source is a source which produces a field which is of compact support. It will then be shown, in Section 3.3, that nonradiating sources do not exist. The physical meaning for the problem considered in this paper of the compactness requirement on the support of the source is that the region of the ionosphere to be probed must be finite.

The derivations of Section 2, and thus the uniqueness proofs of this section, assume that continuous measurements over a closed surface are available (e.g., that S in Equation 4 is closed). The effect of using discrete (discontinuous) measurements over only a portion of the closed surface is to affect the resolution and range of source (ionospheric) structure sizes that can be determined. This is discussed in Section 6 in terms of a band-limiting operation on the set of spatial frequencies recorded and reconstructed in the solution. The identical spatial band-limiting operation can be applied to all steps of all of the uniqueness proofs discussed in this section. The result is that the solution is unique for the measured set of spatial frequencies.

It should be noted that throughout this section any field referred to as being a solution of the wave equation is also assumed to satisfy the Sommerfeld radiation condition.

3.1 THE SCALAR SOLUTION

The uniqueness of the solution to Equation 12 was first deduced by Bojarski (Refs 9,11) and later proven more rigorously by Bleistein and Cohen (Ref 15). A simpler and more physically understandable proof was presented by the author (Ref 16). This proof is presented here.

It is valuable to see intuitively why the measured boundary values should uniquely determine the source term in the wave equation. First consider a point scatterer illuminated by a plane wave (or, equivalently, consider a point radiator), as shown in Figure 1. The scattered field is a spherical wavefront. Now suppose that the boundary values are to be measured over a plane. What information is necessary to uniquely determine the scatterer? Simple geometry shows that the direction of the inward pointing normal and the radius of curvature of the spherical wavefront are sufficient to determine the location of its center, the point scatterer. Elementary geometry also provides that there is sufficient information to uniquely determine these two quantities if the height of the sphere above the measurement plane is known at three noncolinear points in the plane. In electromagnetic terms these heights are simply the relative phases of the spherical wavefront at the three points. Thus, measurement of the relative phase of the spherical wavefront at three noncolinear points in the measurement plane uniquely determines the position of the point source; measurement of the amplitude at these points yields the strength of the scatterer. Now consider the physical meaning of the superposition integral:

$$\phi = \int \rho g \, dV \tag{19}$$

This integral says that the field radiated by an arbitrary source distribution ρ can be represented as the sum of the fields, g, due to each point source in an equivalent point source decomposition of ρ. This, of course, is just a statement of Huygen's principle. By applying the reasoning of this paragraph to each point source and the spherical wave it generates, it becomes obvious that there is enough information present in the scattered field to uniquely determine the source.

The above paragraph is a geometrical interpretation of the detailed and quite rigorous mathematical uniqueness proof given by Bleistein and Cohen (Ref 15). They expanded the source and the fields in orthonormal sets of spheroidal wave functions, and then showed that the measured fields had enough information to determine the coefficients of the set of functions describing the source.

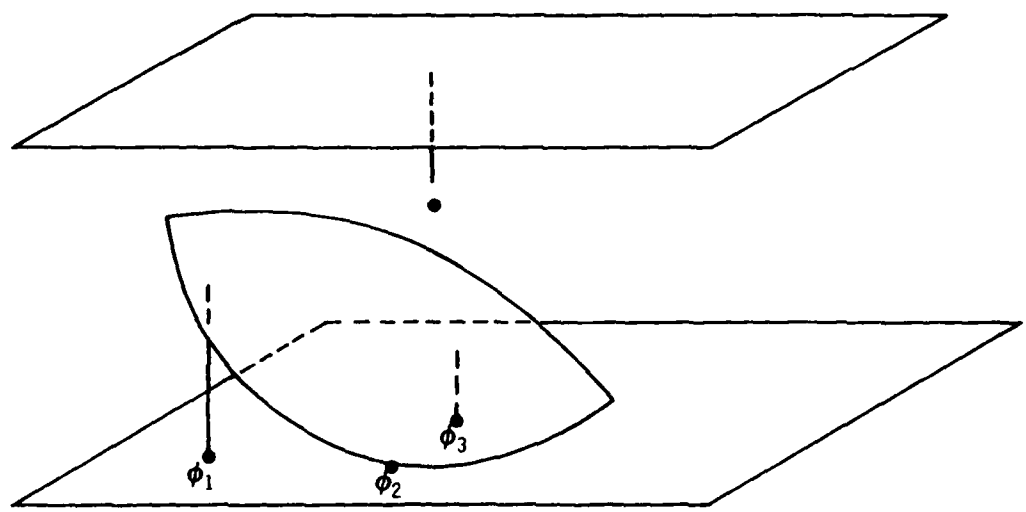

RT-20981

Figure 1. The determination of a point scatterer, illuminated by a plane wave, using measurements of the scattered wave at three noncolinear points in a plane.

The author has presented (Ref 16) a simpler proof by contradiction (reducto ad absurdum) for the uniqueness of the inverse scattering problem. Assume that two different source terms, $\rho_1(\underline{x})$ and $\rho_2(\underline{x})$ (or two different refractive index distributions), produce the same boundry values, $\phi_S(\underline{x})$, on a measurement surface S. This assumption says that the inverse problem is nonunique. It follows from the direct scattering equation that the boundary values due to the two sources are

$$\phi_{S1} = \int \rho_1 \, g \, dV \tag{20}$$

$$\phi_{S2} = \int \rho_2 \, g \, dV \tag{21}$$

The difference between these boundary values over the surface is

$$\begin{aligned} \phi_{SD} &\equiv \phi_{S1} - \phi_{S2} \\ &= \int \rho_1 \, g \, dV - \int \rho_2 \, g \, dV \\ &= \int (\rho_1 - \rho_2) g \, dV \quad , \end{aligned} \tag{22}$$

and

$$\begin{aligned} \phi_{SD} &= \int \rho_D \, g \, dV \\ &= 0 \end{aligned} \tag{23}$$

where ρ_D is the difference between the two sources ($\rho_D \neq 0$ by the original assumption), and $\phi_{SD} = 0$ by the original assumption. Let ϕ_1, ϕ_2, and $\phi_D = \phi_1 - \phi_2$ denote the fields inside S associated with the boundary values ϕ_{S1}, ϕ_{S2}, and ϕ_{SD}, respectively. Because ϕ_1 and ϕ_2 must both satisfy the wave equation, Equation 2, it follows that ϕ_D must also

satisfy the wave equation. Thus ϕ_D is a solution to the wave equation with boundary values which are 0 everywhere on the boundary. By the same argument used to prove the uniqueness of the solution to the wave equation (e.g., Reference 12, Section 9.2), it follows that ϕ_D must be identically zero throughout the bounded volume. But ϕ_D is the (identically zero) solution to the wave equation with source term $\rho_D = \rho_1 - \rho_2$. This means $\rho_D \equiv 0$ through S, which contradicts the original assumption. Thus, the source is uniquely determined by the boundary values.

3.2 THE VECTOR SOLUTION

This subsection extends the author's uniqueness proof for the scalar case to the vector inverse scattering problem.

The proof for vector fields and sources in general, anisotropic media is identical to the scalar proof with two exceptions. First, the Stratton-Chu equations for the field (Reference 12, Section 8.14) must be used in place of the scalar superposition integral. Because the Stratton-Chu equations are linear in the source terms, the steps in the above proof still apply. Second, it is necessary that the result, that zero boundary conditions everywhere over a closed surface imply that the fields are identically zero throughout the bounded volume, hold for fields satisfying the wave equation for general, anisotropic media. Fortunately, this again follows directly from the proof of the uniqueness of the fields in such media. Stratton (Reference 12, Section 9.2) points out why this is so, and Kong (Reference 16, Section 7.1) presents an explicit, rigorous proof.

3.3 NONRADIATING SOURCES

In their proof of the uniqueness of the solution to the inverse scattering problem, Bleistein and Cohen (Ref 15) derive mathematically a class of sources which produce fields that are identically zero everywhere outside a finite volume (i.e., their fields have compact support). Since the fields due to such a source cannot contribute to the boundary values which would be measured outside the volume, it would appear that these sources represent a potential nonuniqueness in the inverse scattering problem. Devaney and Wolf (Ref 18) and Devaney (Ref 19) have also derived and discussed such sources. If such sources did exist physically (as opposed to being derivable mathematically), they would pose little problem for inverse scattering in the context of remotely probing the ionosphere: Nonradiating sources, viewed as induced sources, represent

nonscattering features of the medium. However, they are intellectually bothersome. Fortunately, within the last year, three independent proofs that nonradiating sources cannot exist physically have been obtained.

The first proof was derived by the author (Ref 20) from the realization that fields of compact support are physically inconsistent with the inhomogeneous wave equation. The proof is by contradiction. Assume that $\rho_{NR} \neq 0$ is a nonradiating source which is a proper source term for the wave equation. Further, assume that ρ_{NR} produces a field ϕ_{NR} which is identically zero outside some finite volume V_o. By "produces" it is meant that ϕ_{NR} is the solution to the inhomogeneous wave equation with source ρ_{NR}. Let S be a surface, enclosing a volume V, drawn such that S is completely outside of V_o. Then V_o is contained in V. By the original assumption, ϕ_{NR} is zero everywhere on S. But then ϕ_{NR} is a solution to the wave equation with 0 boundary conditions. It follows, by the uniqueness proof for the solution to the wave equation, that $\phi_{NR} \equiv 0$ throughout V and, in particular, throughout V_{NR}. But then $(\nabla^2 + k^2)\phi_{NR} = 0$ throughout V_{NR}, and $\rho_{NR} \equiv 0$ throughout V_{NR}. This contradicts the original assumption. This proof would fail if the particular frequency involved happened to be an eigenfrequency for the volume V, except that the conditions must be true simultaneously for all possible volumes containing V_{NR}, and all surfaces surrounding V.

The second proof was obtained by the author during the course of the research reported in this paper. The basic form of the exact analytic solution for the fields in the inverse scattering problem obtained by Bojarski (see Section 4) is an expression which shows that the spatial Fourier transform of the field, $\tilde{\phi}(\underline{k},\omega)$, is given by $\tilde{\theta}(\underline{k},\omega,v)$, evaluated at $v^2 = \omega^2/k^2$ (on the Ewald sphere, in the terminology of Section 4). It is also shown in Section 4 that the Fourier transform of the field is identically zero for $v^2 \neq \omega^2/k^2$. This means that the spatial Fourier transform of the field is of compact support. It is a well-known property of the Fourier transform (c.f. Reference 21, pp. 143 ff) that if the transform of a function has compact support, then the function cannot have compact support. It follows that fields which are proper solutions of the inhomogeneous wave equation cannot be of compact support. Since the compactness of the support of the fields produced by a nonradiating source is a necessary condition for the existence of such sources, this means nonradiating sources cannot exist.

The third proof was suggested by N. N. Bojarski (Ref 22). In a recent paper, Porter and Devaney (Ref 23) prove that the solution to the inverse source problem which possesses minimum source energy is the solution in which any nonradiating part is

zero. Bojarski has pointed out that the physical meaning of Lenz's law is that currents and charges always assume the minimum energy distribution. Hence, any nonradiating source contribution is zero.

In summary, the solution to the inverse scattering problem is unique, in both the scalar and the vector cases.

4. EXACT, CLOSED-FORM, ANALYTIC SOLUTIONS FOR THE TOTAL FIELD AND THE SOURCE

4.1 THE SOLUTION FOR THE FIELD (Refs 24,25)

In the derivation of Section 2.1, Equations 9 and 10 were arrived at as two simultaneous equations in two unknowns: The sources, ρ, and the total field, ϕ. It was chosen to eliminate ϕ and solve for ρ. Bojarski has shown (Ref 25) that by starting with a slightly different form of the initial equations and eliminating ρ instead of ϕ, it is possible to obtain a closed-form, analytic solution for the total field, ϕ.

The derivation begins with a somewhat more general form of the wave equation

$$\nabla^2\phi(\underline{x},\omega) + \left[\omega^2/c^2(\underline{x},\omega)\right]\phi(\underline{x},\omega) = -\rho(\underline{x},\omega) \tag{24}$$

where ω is the temporal frequency (which will often be suppressed in this section), and c is a velocity which varies as a function of both $\underline{x}$ and ω. If the constitutive equation is written as

$$\rho_t(\underline{x},\omega,v) = \left\{\left[\omega^2/c^2(\underline{x},\omega)\right] - \omega^2/v^2\right\}\phi + \rho(\underline{x},\omega) \tag{25}$$

where v is an arbitrarily chosen constant "free space" reference velocity, then Equation 24 can be written as

$$\nabla^2\phi(\underline{x},\omega) + \left[\omega^2/v^2\right]\phi(\underline{x},\omega) = -\rho_t(\underline{x},\omega,v) \tag{26}$$

ρ_t is introduced to permit writing Equation 30 with a constant coefficient in front of ϕ. If G is the Green's function associated with the constant reference velocity, v, then G satisfies Equation 26 with a delta function source. Note that G satisfies Equation 26, and not Equation 24.

Let a quantity θ be defined as

$$\theta \equiv \oint d\underline{S} \cdot (G_r \nabla\phi - \phi \nabla G_r) \tag{27}$$

where G_r = ReG, which also satisfies Equation 26 with a delta function source. θ is analogous to ϕ_H of Equation 4, and has many of the same properties. In particular, θ depends only on the measured data, and is thus known. If the same steps that were carried out in going from Equation 4 to Equation 9 are applied to Equation 27, the following integral equation is obtained:

$$\theta = \phi - \int dV\, G_r \rho_t \tag{28}$$

Equations 9 and 28 are quite similar.

Let a new source term ρ_γ be introduced which has support only over the volume of integration V:

$$\rho_\gamma(\underline{x},\omega,v) \equiv \begin{cases} \rho_t(\underline{x},\omega,v) & , \ \underline{x} \in V \\ 0 & , \ \underline{x} \notin V \end{cases} \tag{29}$$

Then Equation 28 can be written as

$$\theta(\underline{x},\omega,v) = \phi(\underline{x},\omega) - \int_{-\infty}^{\infty} G_r(\underline{x}|\underline{x}',\omega,v)\, \rho_\gamma(\underline{x}',\omega,v) d^n x' \tag{30}$$

In Cartesian coordinates G_r is a difference kernal and the integral in Equation 30 becomes a convolution. Using superscript tildes to denote the n-dimensional spatial Fourier transform of quantities, the spatial Fourier transform of Equation 30 becomes

$$\tilde{\theta}(\underline{k},\omega,v) = \tilde{\phi}(\underline{k},\omega) - \tilde{G}_r(k,\omega,v)\tilde{\rho}_\gamma(\underline{k},\omega,v) \tag{31}$$

where $\underline{k}$ is the transform variable. Note that ϕ and its spatial Fourier transform cannot depend on the arbitrary reference velocity v.

The spatial Fourier transforms of the real and imaginary part of the Green's function are

$$\tilde{G}_r(\underline{k},\omega,v) = P\, 1/(k^2 - \omega^2/v^2)$$

$$= \begin{cases} 1/(k^2 - \omega^2/v^2) , & k^2 \neq \omega^2/v^2 \\ 0 , & k^2 = \omega^2/v^2 \end{cases}$$

$$\tilde{G}_i(\underline{k},\omega,v) = (\pi/2k)\left[\delta\left(k - \frac{\omega}{v}\right) - \delta\left(k + \frac{\omega}{v}\right)\right] \tag{32}$$

where $k = |\underline{k}|$ and P denotes the principal value. Note that the support of $\tilde{G}_r$ is everywhere except on the sphere $k^2 = \omega^2/v^2$, and the support of $\tilde{G}_i$ is only on the sphere $k^2 = \omega^2/v^2$. This sphere is termed the Ewald sphere. Note also that the spatial Fourier transform of G is invariant with respect to the dimensionality of the space. Because the support of $\tilde{G}_r$ is everywhere except on the Ewald sphere,

$$\tilde{G}_r(\underline{k},\omega,v)\Big|_{v=\omega/k} = \tilde{G}_r(\underline{k},\omega,\omega/k) = 0 \tag{33}$$

If Equation 31 is evaluated for $v^2 = \omega^2/k^2$ (on the Ewald sphere), then, by Equation 33,

$$\tilde{\theta}(\underline{k},\omega,\omega/k) = \tilde{\phi}(\underline{k},\omega) \tag{34}$$

Taking the inverse spatial Fourier transform of Equation 34 yields

$$\phi(\underline{x},\omega) = (1/2\pi)^n \int_{-\infty}^{\infty} e^{-i\underline{k}\cdot\underline{x}} \tilde{\theta}(\underline{k},\omega,\omega/k)\, d^n k \tag{35}$$

This is an exact, closed-form analytic solution for the total field, ϕ. Note that ϕ does not depend on the arbitrary reference velocity, v, used in the Green's function, since ϕ must satisfy Equation 24, which is independent of v.

Previous solutions to the inverse scattering problem have yielded expressions for the source which were dependent on the velocity used in the Green's function. Without additional information, determination of the source off the Ewald sphere surface is precluded. The author (Ref 26) has shown that the requirement that the source be of compact (finite) support is both necessary and sufficient additional information. However, the solution given by Equation 35 achieves the same effect in an elegant fashion. As the free parameter v is varied, the Ewald sphere on which $\tilde{\theta}$ is evaluated sweeps throughout spatial Fourier transform space to obtain the complete spatial reconstruction of $\phi(\underline{x})$.

A more complete derivation of these results is given in Bojarski (Ref 25).

4.2 THE SOLUTION FOR THE SOURCE

This result is perhaps the most important result obtained by the author in the course of the research reported in this paper.

A major advantage of solving the inverse scattering problem using numerical solution of the integral equation, Equation 12, as discussed in Section 2, is that fast Fourier transform (FFT) techniques can be employed. This makes treatment of three-dimensional, real-world problems well within standard computer capabilities. However, numerical evaluation of Equation 35 is not necessarily as efficient, because of the problems associated with evaluating $\tilde{\theta}$. Furthermore, although Bojarski (Ref 25) has shown that by evaluating the Laplacean of Equation 35 in the Fourier domain (using the Fourier differentiation theorem) an expression for the source can be obtained, it would be preferable to have an expression for the source directly in terms of the measured data.

The author has derived two results presented here. First, an expression for $\tilde{\theta}$ in terms of Fourier transform operations on the measured fields is presented. This makes numerical evaluation of the solution for the fields using FFT's possible. Second, an expression for the source in terms only of $\tilde{\theta}$ (and thus the measured data) is obtained.

Bojarski (Ref 25) has pointed out that since on the Ewald sphere shell $G_r = 0$, for this case

$$\theta = -\oint d\underline{S} \nabla G_r \phi \tag{36}$$

This avoids the requirement to evaluate $\nabla\phi$ over the measurement surface, which is quite desirable when the measured field contains noise. Consider the case where the measurement surface is the x-y plane (more general, nonplanar surfaces can be accommodated using the same formulation by adjusting the phase at each measurement point such that the measured data is the same as if it had been measured over a plane). Then Equation 36 becomes (ω and v are temporarily suppressed)

$$\theta(x,y,z) = -\int dx'dy' \, \phi(x',y',0) \, \partial/\partial z \, G_r(x-x',y-y',z) \tag{37}$$

Evaluation of Equation 37 using numerical integration requires spatially sampling ϕ on the measurement surface at an interval small compared to oscillations in G_r, and thus small compared to a wavelength. This is impossible in most real-world situations; numerical integration is also slow. These limitations can be avoided by evaluating θ in the Fourier transform domain, using FFTs. This requires an analytical expression for the two-dimensional spatial Fourier transform of the normal derivative of G_r. Noting that $2G_r = G+G^*$, this reduces to evaluating $1/2\ \partial/\partial z\ (G+G^*)$. Harrington (Ref 27) derives the following expression for G^*:

$$\frac{e^{-iqr}}{r} = (-i/2\pi) \int_{-\infty}^{\infty}\int e^{i2\pi(\nu_x x+\nu_y y)}\ \frac{e^{-iz\sqrt{q^2-(2\pi\nu_x)^2-(2\pi\nu_y)^2}}}{\sqrt{q^2-(2\pi\nu_x)^2-(2\pi\nu_y)^2}}\ d(2\pi\nu_x)d(2\pi\nu_y) \tag{38}$$

where $q \equiv \omega/v$ and $r = (x^2 + y^2 + z^2)^{1/2}$. Taking the derivatives of both sides of Equation 38 with respect to z and applying the definition of the Fourier transform yields

$$\begin{aligned} \mathcal{F}_{xy}\left\{\partial/\partial z\ G^*\right\} &= \mathcal{F}_{xy}\left\{\partial/\partial z\ \left(\frac{e^{-iqr}}{4\pi r}\right)\right\} \\ &= (-1/2\pi)e^{-iz\sqrt{q^2-(2\pi\nu_x)^2-(2\pi\nu_y)^2}} \end{aligned} \tag{39}$$

Sherman (Ref 32)gives

$$\begin{aligned} \mathcal{F}_{xy}\left\{\partial/\partial z\ G\right\} &= \mathcal{F}_{xy}\left\{\partial/\partial z\ \left(\frac{e^{iqr}}{4\pi r}\right)\right\} \\ &= (-1/2\pi)e^{\ iz\sqrt{q^2-(2\pi\nu_x)^2-(2\pi\nu_y)^2}} \end{aligned} \tag{40}$$

$\mathcal{F}_{xy}$ denotes the two-dimensional spatial Fourier transform from x,y to ν_x, ν_y.

Equation 37 is a convolution in x and y. It follows, using Equations 39 and 40 and the convolution theorem that

$$\theta(x,y,z,\omega,v) = \mathcal{F}_{xy}^{-1}\left\{\mathcal{F}_{xy}\{\phi(x,y,0,\omega)\}\, P(\nu_x,\nu_y,z,\omega,v)\right\} \tag{41}$$

where

$$P(\nu_x,\nu_y,z,\omega,v) = (1/4\pi)\, e^{-iz\sqrt{q^2-(2\pi\nu_x)^2-(2\pi\nu_y)^2}} + e^{iz\sqrt{q^2-(2\pi\nu_x)^2-(2\pi\nu_y)^2}} \tag{42}$$

This expression is strictly valid for $v = \omega/k$. A similar expression, involving an additional term of the same form as in Equation 41, has been derived for $v \neq \omega/k$.

The importance of Equation 41 is that it permits evaluating θ (and thus $\tilde{\theta}$) using FFTs. Indeed, the algorithm is quite simple:

1. Compute the two-dimensional spatial Fourier transform of the measured field data, $\theta(x,y,0)$, using an FFT.
2. Multiply, in the spatial frequency domain, by the "propagator" function, P, given in Equation 42.
3. Compute the two-dimensional inverse spatial Fourier transform of the product, using an FFT.

This method of evaluating $\tilde{\theta}$ is analogous to the Fourier domain method often used for reconstructing holograms (c.f. Section 6), and for evaluating the Kirchhoff integral (Ref 28).

Given an efficient means of computing θ, the evaluation of ϕ becomes equally efficient. To obtain an equally efficient expression for the source term, ρ_γ, substitute Equation 32 into Equation 31. Requiring that $k \neq \omega/v$, this yields

$$\tilde{\theta}(\underline{k},\omega,v) = \tilde{\Phi}(\underline{k},\omega) - (k^2-\omega^2/v^2)^{-1}\, \tilde{\rho}_\gamma(\underline{k},\omega,v) \tag{43}$$

Substituting Equation 34 into Equation 43 and carrying out some algebra gives

$$\tilde{\rho}_\gamma(\underline{k},\omega,v) = \left[\tilde{\theta}(\underline{k},\omega,\omega/k) - \tilde{\theta}(\underline{k},\omega,v)\right](k^2-\omega^2/v^2) \tag{44}$$

Equation 44 is an exact, closed-form analytic solution for the source term in the inverse scattering problem. Physically, it says that ρ_γ can be written as the difference between the θ field on the Ewald sphere and the θ field off the Ewald sphere. Although they will not be repeated here, all of the results in the other sections of this paper concerning the nonexistence of nonradiating sources, the effects of incomplete measurements and noise, the well-posedness of the solution, etc., can be deduced from this analytic solution.

5. SIMULATION

At the start of this research, one goal was to carry out a reasonably realistic two- or three-dimensional numerical or analytical simulation of the determination of the refractive index profile using the inverse scattering techniques of Section 2. This goal was arrived at based on the assumption that analytical and/or numerical methods for computing the necessary directly scattered fields were available. Such methods are a necessary prerequisite for any simulation, since the fields produced by the interaction of a probing wave as it propagates through the ionosphere represent the (simulated) "measured" data used as input to the inverse scattering solution. As it turned out, the research tested this hypothesis, and found that such methods did not really exist. This, coupled with the resources devoted to the very important and unforeseen analytical results presented in Section 4, resulted in only partial accomplishment of the simulation goal. However, four substantial and very useful results were obtained:

1. The numerical solution to the inverse scattering integral equation of Section 2 was implemented for the two-dimensional case. In the process, several preliminary results concerning a very broad class of deconvolution problems were obtained.

2. Both numerical and analytical simulations employing the Epstein profile were attempted. It was finally realized that this approach is not applicable to a trans-ionospheric experiment, and the reasons for this were determined. Based on rather extensive discussions with workers in the ionospheric propagation field, the author believes that this point is not well known.

3. A method for calculating the required directly scattered data, to use as input to the inverse scattering simulation, was developed. Its implementation was completed, but its testing was not.

4. To demonstrate the features that should be obtainable with the inverse scattering technique of Section 2, a one-dimensional simulation was implemented. This employed a time domain direct and inverse scattering theory that can be viewed as analogous to the theory presented in Section 2. Results

were obtained for quite realistic one-dimensional ionospheric profiles. The ability to obtain accurate determination of the profile between local maxima and above the absolute maximum of the electron density, using only data that could be obtained with a single, vertical incidence sounder operating on the ground, was demonstrated. This has the potential for direct application to the processing of existing ionospheric sounder data

The above results are reported in Sections 4.1 through 4.4, respectively. Finally, it is pointed out in Section 4.5 that a recent result of the author's (presented in Section 6) shows that, under conditions that would probably be employed in a practical ionospheric experiment, results from previous numerical and experimental work achieved the currently desired simulation goal in a manner not previously recognized.

5.1 NUMERICAL SOLUTION TO THE INVERSE SCATTERING PROBLEM

It was shown in Sections 2.2 and 2.3 that solving the inverse scattering problem to obtain the electron density distribution consists of five steps. The first step is to solve the basic integral equation, Equation 12, for the source, $\rho(\underline{x})$. The subsequent four steps are *straightforward to implement; this first step is not.*

In two dimensions, Equation 12 is written in discrete form as follows:

$$\phi_H(\ell,m) = \sum_{p=-N+1}^{N-1} \sum_{q=-M+1}^{M-1} h(\ell-p,m-q)\rho(p,q) \tag{45}$$

where h is Img, and discrete indices have been substituted for Cartesian variables, implying (usually uniform) sampled, discrete values. Thus, $\phi_H(\ell,m)$ is the complex value of ϕ_H at x_ℓ, y_m within the N by M set of x,y points at which ϕ_H is known. ϕ_H and ρ in Equation 45 are two-dimensional N by M matrices. h is a block, or vector, Toeplitz matrix. A comprehensive discussion of Toeplitz matrices is given in Reference 29. A Toeplitz matrix is a matrix in which elements along each left-to-right diagonal are the same. A block Toeplitz matrix consists of submatrix blocks which are Toeplitz, arranged in turn in Toeplitz fashion (as shown in Equations 46 through 49, below). It can be shown that a matrix will have this property if matrix elements for which the *difference in the row, column indices is the same* have the same value. Because the Green's function depends only on the difference of the coordinates, the discrete matrix representation of Img has this property. Indeed, any two- or three-dimensional convolution relationship leads to an equation of the form of Equation 45. Because of

this, several of the results obtained below can be applied to any linear system in which the output is expressable in terms of the convolution of the input with an "impulse response" function.

Equation 45 can be written in matrix notation as follows (a single underline denotes a column vector; a double underline denotes a matrix).

$$\underline{\phi}_H = \underline{\underline{h}}\,\underline{\rho} \tag{46}$$

where

$$\underline{\underline{h}} = (h^{p-q}) \quad 0 \leqslant p,q \leqslant N-1, N \geqslant 1 \tag{47}$$

$$\underline{\underline{h}}^r = (h^r_{p-q}) \quad 0 \leqslant p,q \leqslant M-1, M \geqslant 1 \tag{48}$$

and

$$h^r_s = h(r,s) \tag{49}$$

In forming the MN dimensional column vectors $\underline{\phi}_H$ and $\underline{\rho}$, the first N elements of $\underline{\phi}_H$, for instance, are the elements of the first row of $\phi_H(\ell,m)$, the next N elements are from the second row, etc., for M rows.

Equation 46 can be solved for $\underline{\rho}$ by inverting the matrix $\underline{\underline{h}}$. This procedure was implemented, using a standard, very well written double precision complex matrix inversion routine which employed Gaussian elimination with pivoting and equilibration. The resulting routine was tested using various combinations of delta function source terms, and the associated values of ϕ_H computed by direct evaluation of Equation 45. The solutions for ρ were accurate to full single precision machine accuracy when single precision values of ϕ_H were employed and no simulated measurement noise was added to ϕ_H. The fact that a double precision matrix inversion routine is required to yield single precision accuracy is due to two causes. First, Gaussian elimination with pivoting, even with equilibration, suffers from a significant loss of precision unless the matrix being inverted is very well conditioned. Although this has been known in numerical analysis circles for many years (c.f. Ref 30), very few computer routines consider the conditioning of the matrix, and almost none apply the required iterative

improvement techniques (Ref 30). This is true in spite of the fact that a properly written routine which employs iterative improvement can readily yield single precision accuracy for the inverse using only single precision elimination, pivoting, and other computations. Only after considerble effort, and only as this paper is being written, was the author able to obtain a proper inversion routine employing iterative improvement.

The inherent ill-posedness of Equation 45 when h is derived from the free space Green's function (or its imaginary part) is well known. It is a result of the many powers of 10 variation in the numerical values of h which occur when propagation distances larger than a few wavelengths are involved. Fortunately, the solution to Equation 45 has been shown by the author, both numerically and analytically, to be rendered well-posed when certain a priori information is employed in solving for it. This is true even in the presence of measurement noise in ϕ_H (see Section 6). The primary piece of information necessary to obtain this well-posedness is the fact that the source is of compact support. Since solutions over finite volumes utilizing data measured over finite apertures are all that are sought in any real-world situation, this information is always available.

To summarize, the ability to numerically solve Equation 12 for the source term was demonstrated. The behavior in the presence of noise was consistent with previous results, as discussed in Section 6. Extensive experimentation with the behavior of the discrete form of Equation 12 was limited by the unavailability of a proper matrix inversion routine. Such a routine has now been obtained, and is available for future work.

In the process of examining the numerical behavior of equations of the form of Equation 45, several additional but preliminary results were obtained. Because Equation 45 has broad application to almost any linear physical system, these results deserve pursuit in future work (although not necessarily as a part of additional research on the ionospheric profiling problem).

As a part of the process of understanding the numerical properties of Equations 12 and 45, the author carried out in-depth research on the inversion of block Toeplitz systems in the presence of noise. The following paragraphs summarize this work.

Many papers on the inversion of Toeplitz systems have appeared. However only a relatively few of these deal with block Toeplitz systems, and are thus applicable to two- and three-dimensional problems. The inversion of block Toeplitz matrices is accomplished via one of two general approaches: Approximation via a circulant matrix

and inversion using fast Fourier transform (FFT) methods, or direct inversion taking advantage of the symmetry. The approach chosen has very important implications for both efficiency and accuracy.

Real-world measurements can involve anywhere from 32 by 32 data arrays to arrays of several hundred square. The inversion time depends on the product of the dimensions (or the total number of elements) of the Toeplitz matrix. Let this quantity be L (=1024 for a 32 x 32 matrix). Standard matrix inversion techniques require times proportional to L^3 with, for example, one minute of execution required for L = 256, but over an hour required for a 32 x 32 matrix on a VAX 11/780. (These times are based on the requirement to use double precision, as discussed above. A factor of ten or more savings should be realized by going to single precision methods using iterative improvement.) Algorithms which take advantage of the symmetry of a Toeplitz matrix have reduced this over the last decade to a constant times L^2. The reader can assess this progression and the current status of such algorithms by consulting References 31 through 42. Many of the published algorithms have not been implemented, or their implementations are not applicable to the solution of Equation 45. In short, no "direct" inversion algorithm which exploits the structure of a Toeplitz matrix and which is applicable to block Toeplitz forms could be found. Furthermore, the behavior of these algorithms in the presence of ill-conditioning and noise is largely unknown.

One very promising development has occurred in this field during the period of this research. Three groups, working independently, have developed algorithms which claim to invert Toeplitz matrices in times of order $L \log^2 L$ (Refs 43-46). Unfortunately, discussions with at least one author from each of the three groups have established that as of July 1981 none of the algorithms has been implemented for Toeplitz systems, let alone for block Toeplitz matrices. It is anticipated that a block Toeplitz routine may be available circa January 1982.

As this paper was being written, the author was able to obtain a routine written by S. Wood (Ref 47) (who did her Ph.D. under M. Morf--c.f. Ref 43) which provides a partial implementation of these methods for block Toeplitz matrices. There has been no opportunity to examine this routine in detail.

A circulant matrix is a matrix in which the elements of each row are the elements of the previous row, right-circularly-shifted one position. Circulant matrices can be inverted in order $L \log_2 L$ operations, because their eigenvalues can be obtained by computing the discrete Fourier transform of a single row or column. Toeplitz matrices

play a fundamental role in digital image processing and restoration. However, the minimum size matrix of interest for such applications tends to be of order 256 x 256, or larger. This has led to extensive development of fast approximate techniques for inversion, based on the approximation of the Toeplitz matrix by a related circulant matrix. Reference 43 (Chapters 7 and 8) and Reference 44 (Chapter 5) review such techniques in detail, as well as providing over two dozen references used by the author. The fundamental problem in applying these techniques to the inverse scattering problem is that, although the Fourier transform operations tend to improve the inversion over other methods in the presence of ill-conditioning, the approximation of the original Toeplitz matrix introduces significant errors. This is in part due to the rather heurestic methods used to arrive at the circulant approximation of the Toeplitz matrix (an infinity of such approximations exist for any particular Toeplitz matrix). There are two interesting exceptions to this, however.

Gray showed (Ref 50) that the eigenvalues of a finite Toeplitz matrix and certain of its circulant approximations are asymptotically equal. In a paper that has apparently been almost totally overlooked by the community dealing with Toeplitz matrices, Ekstrom (Ref 51) combined this choice of circulant approximation with an iterative improvement method (such as discussed above) and applied the result to the inversion of block Toeplitz matrices. The result has an execution speed of the order of the FFT within each iteration, and appears to be capable of handling ill-conditioned matrices. There was insufficient time remaining to implement Ekstrom's algorithm by the time the basis for its operation and its significance were understood by the author. However, this approach should receive high priority in future work.

Equation 45 is a two-dimensional convolution equation. It can be solved using FFT techniques. Let $\mathcal{F}$ and $\mathcal{F}^{-1}$ denote the direct and inverse discrete Fourier transform of a quantity, respectively. Then the solution to Equation 45 can be computed as

$$\rho = \mathcal{F}^{-1}\left\{\mathcal{F}[\phi_H]/\mathcal{F}[h]\right\} \tag{50}$$

The problems of using Equation 50 when ϕ_H contains noise and when the Fourier operations are indeed discrete (and therefore approximate) are discussed in detail in Reference 48 (Sections 6.1 and 6.2) and Reference 49 (Section 5.3.1 ff). It has been shown by this author that the approach of Equation 50 can be made well-posed by applying constraints using a priori information that is always available (Refs 52,53).

However, a general algorithm for applying these constraints is not yet available. Hunt (Ref 54; Ref 48, pp. 148-50 ff; Ref 49, Section 5.6) has developed an algorithm for image restoration which carries out the processing of Equation 50 using a constrained least-squares method in which the constraint utilizes information on the statistics of the noise in the data which would be available in any practical inverse scattering experiment. In one sense, it can be proven that this method yields the best solution obtainable in the presence of noise. There is also a close connection between the method of applying the constraint in Hunt's algorithm and the method employed by the author in proving the above-mentioned results on well-posedness. This approach should also be seriously examined in future work.

5.2 INVESTIGATIONS OF DIRECT SCATTERING SIMULATION USING EPSTEIN AND RELATED PROFILES

A significant amount of work has been carried out modeling ionospheric propagation using Epstein and related profiles. These are profiles which vary in one dimension according to an analytical formula. The formula for the profile appears in the coefficient multiplying the field in the wave equation. By proper choice of the analytic form of the profile, the wave equation takes the form of an equation that can be solved analytically in terms of known functions. Usually, a profile involving the hyperbolic trigonometric functions is used, and the wave equation is transformed into the hypergeometric equation. Examples of this approach which were examined in depth during this research are contained in References 55 through 69. Books by Brekhovskikh (Ref 70) and Wait (Ref 71) treat this topic in detail. This approach appears, at first glance, to be ideal for computing the direct scattering data to be used as input to an inverse scattering simulation. It gives an analytic solution. There are two problems, however: The approach is one dimensional, and it applies to reflection problems only.

A two-dimensional problem of interest can be treated using the same mathematics by employing a point source as the illumination. Although most of the one-dimensional problems treated in the literature assume plane wave illumination incident normally on the medium, solutions for a plane wave at an arbitrary angle of incidence are available. The point source can then be expanded into an angular spectrum of plane waves, and the arbitrary angle of incidence solution applied to each spectral component. This analysis was carried out and implemented on the computer.

At this point a subtle aspect of the analysis for Epstein-type layers was identified. All of the profiles employed in all of the available analytic solutions extend to infinity. Half-space problems can be treated by using a profile that is symmetric about the

origin, but the profile is still infinite in one direction. In the ionospheric inverse scattering problem, it is necessary to have the source a finite distance from the measurement surface (e.g., the satellite must be at finite altitude). If this is not the case, then only a single plane wave illuminates the ionosphere. Furthermore, the scattering and measurements occur in the far field of the source, which implies that the relative phase of the unscattered component of the wave illuminating the ionosphere at various altitudes is the same. The result is the loss of the ability to resolve height information using a single frequency. Using the analytic profile method, the geometries which can be treated for a semi-infinite profile with the receiver in the free space portion (such as is the case for the problem being modeled here) are limited to those in which the source is at infinity, or in which the source is in the same half-space as the receiver (the backscatter case). Truncation of the profile at a finite distance renders the analytic solution invalid. It is possible to obtain normal mode solutions in a geometry involving a truncated analytic profile, but the full, continuous spatial spectrum is required.

Two other, related techniques were also briefly considered. Numerical ray tracing programs exist for the ionosphere with arbitrary profiles. However, ray tracing is valid only in the geometrical optics limit. Solutions exist for propagation through finite media consisting of discrete layers. Unfortunately, reflections are generated from the artificial boundaries between the layers. It was recognized a little over a decade ago that this effect rendered such solutions for ionospheric problems invalid unless the layer thickness was small both compared to the distance over which the profile varies and compared to the wavelength. This latter requirement makes the number of computations required impractical for the cases of interest here.

5.3 SPATIAL FREQUENCY DOMAIN METHODS FOR DIRECT SCATTERING SIMULATION

When the assumption, that analytic solutions for such profiles as the Epstein profile could be used to simulate the required direct scattering data, proved false, other methods were investigated. The required technique must be efficient, since substantial data sets are involved. It must be applicable to two- and three-dimensional problems, and preferably to media varying in two and three dimensions. It must handle problems with finite distances between source and receiver, and in which forward scattering is important. Finally, techniques based on approximations to the scattering or diffraction processes are less than ideal, since the purpose is to test an exact inverse technique.

One approach is to solve the wave equation numerically, using finite difference or finite element methods. This is probably not adequately efficient, and would be quite difficult to implement.

A technique which satisfies the above criteria was developed by Bojarski (Ref 72), who termed it the "k-space" method. A simulation begins by specifying the electron density as a function of the spatial coordinates, and thus determining the refractive index. It is desired to compute the fields on the ground, due to the source of the probing field, in the presence of this spatially varying refractive index. To compute the fields the wave equation, Equation 2, must be solved. However, the refractive index enters via Equation 3, which in turn depends on the field. Thus, these two equations must be solved simultaneously. Bojarski noted that in $\underline{x}$ space Equation 2 is a differential convolution equation, while Equation 3 is algebraic. Conversely, in Fourier transform space (or "$\underline{k}$" space in Bojarski's notation), Equation 2 is algebraic, while Equation 3 is a convolution equation. He then devised an iterative technique which alternates between the two spaces, solving each equation in the domain where it is algebraic. Because FFTs are used to go back and forth between the two domains, the solution is obtained quite efficiently. Often, only a few (<10) iterations are necessary. Kruger (Ref 73) applied this technique to several two-dimensional problems.

The k-space technique was implemented by the author. However, problems were encountered with convergence of the iterations using realistic ionospheric refractive index distributions. A simpler, noniterative version, used previously by the author to simulate the Holographic Radio Camera experiment (Ref 5), was then implemented. (After the author developed it, it was recognized that this method is essentially equivalent to the first iteration of Bojarski's technique). It models the ionosphere as made up of homogeneous cells, large compared to a wavelengtgh. Propagation through each cell is computed by using the analytical spatial Fourier transform of the Green's function for a homogeneous medium with the properties of the cell, multiplying by the numerical spatial Fourier transform of the field incident on the cell, and computing the inverse numerical Fourier transform of the result. This is a Fourier domain method of evaluating Equation 10 (the solution to Equation 2) without having to sample at an interval small compared to a wavelength. Preliminary results indicate that this method is quite efficient, and may be accurate enough to provide the needed simulated data.

Very recently Kastner and Mittra (Refs 74,75) have presented a modified version of Bojarski's k-space method which they call the "spectral domain" method. The relationship between the two methods can be seen by considering a two-dimensional

problem. In the k-space method, two-dimensional Fourier transforms are employed, and consistency between Equations 2 and 3 is enforced once per iteration. In the spectral domain method, a series of one-dimensional transforms is taken to propagate the field in the second dimension (as in the author's approach). However, the consistency between Equations 2 and 3 and satisfaction of the boundary values is enforced at each cell boundary--many times per iteration. The author thinks it is likely that this will eliminate the convergence problems mentioned above. Discussions with Mittra (Ref 76) confirm that the spectral domain method has been used successfully on two-dimensional inhomogeneous dielectric media. This technique should receive first priority in future work.

5.4 RESULTS OF ONE-DIMENSIONAL TIME DOMAIN INVERSE SCATTERING SIMULATION

As a means of demonstrating the quality of electron density distribution reconstructions which should be possible using inverse scattering techniques, a one-dimensional simulation was carried out. It was also felt that the technique employed might have direct application to the processing of data from existing vertical incidence sounders. This has proven to be the case.

The method used is an efficient "stepping in time" technique developed by Bojarski (Ref 77). The equations are given in his paper. As applied to obtain the results shown below, an impulsive plane wave is assumed to be incident vertically from below on an ionosphere which has a vertical variation in electron density such as is shown in Figure 2. The horizontal axis is normalized; the "F-region" peak corresponds to a density of 3×10^8 electrons/m^3. The corresponding value for the bottom of the "E-region" ledge is 7×10^6 e^-/m^3, and the value at 1000 km altitude is 3×10^6 e^-/m^3. This is a reasonably typical daytime profile. The time history of the reflection coefficient is computed. Noise is added by specifying a fraction of the peak magnitude of the reflection coefficient, and then for each time sample computing a pseudorandum number in the range of zero to this fraction of the peak which is added to the reflection coefficient at that time. This noise-contaminated reflection coefficient is then employed in the inverse scattering algorithm to reconstruct the profile. The maximum deviation and the root mean square deviation between the true and reconstructed profile are also computed.

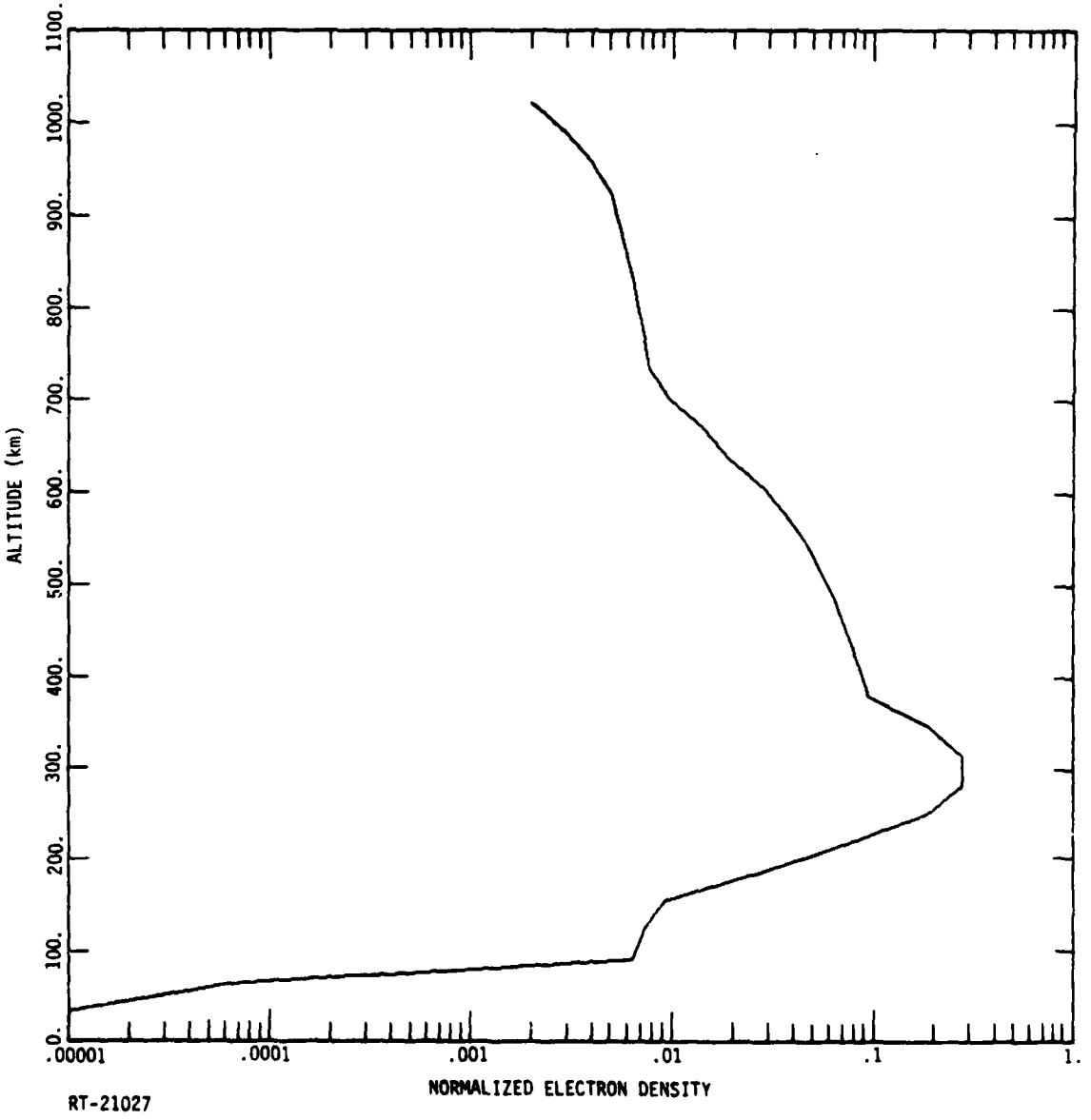

Figure 2. Normalized electron density profile used for time domain inverse scattering simulation.

Figures 3 through 8 show the results for various amounts of noise. Quantitatively, these results can be summarized as follows (single precision--6-1/3 digit--computations were used):

Noise fraction of Peak Reflection Coefficient	Maximum Deviation	RMS Deviation
0	2.98×10^{-8}	1.08×10^{-8}
1.0×10^{-2}	1.07×10^{-2}	4.82×10^{-3}
5.0×10^{-2}	5.17×10^{-2}	2.26×10^{-2}
1.0×10^{-1}	9.75×10^{-2}	4.17×10^{-2}
1.5×10^{-1}	1.36×10^{-1}	5.75×10^{-2}
2.0×10^{-1}	1.67×10^{-1}	7.07×10^{-2}

Several things are significant about these results. First, the maximum deviation and the rms deviation are both bounded by the noise fraction. This is consistent with the results of the author for the Exact Theory (see Section 6). However, it is in sharp contrast with the results obtained and the conclusion drawn, with respect to stability in the presence of noise, by Bojarski (Ref 77). The author postulates that this is because Bojarski employed a profile with a large discontinuity in it. It would be valuable to perform further numerical experiments and analysis to test this postulate. Second, the profile above the maximum is reconstructed from only bottom-side data. Without resorting to incoherent scatter radar, the author knows of no other technique which permits determination of the profile above the peak using only bottom-side illumination and measurements. Third, it appears that this same data processing can be directly applied to existing vertical incidence sounders. The Digisonde appears to be ideal for this.

5.5 APPLICABILITY OF THE HOLOGRAPHIC RADIO CAMERA RESULTS AS A SIMULATION OF THE CURRENT PROBLEM

In Section 6 it is shown that, in the limit where the wavelength of the probing radiation is short compared to all distances in the problem and compared to any medium variations to which the measurement is sensitive, the holographic reconstruction is

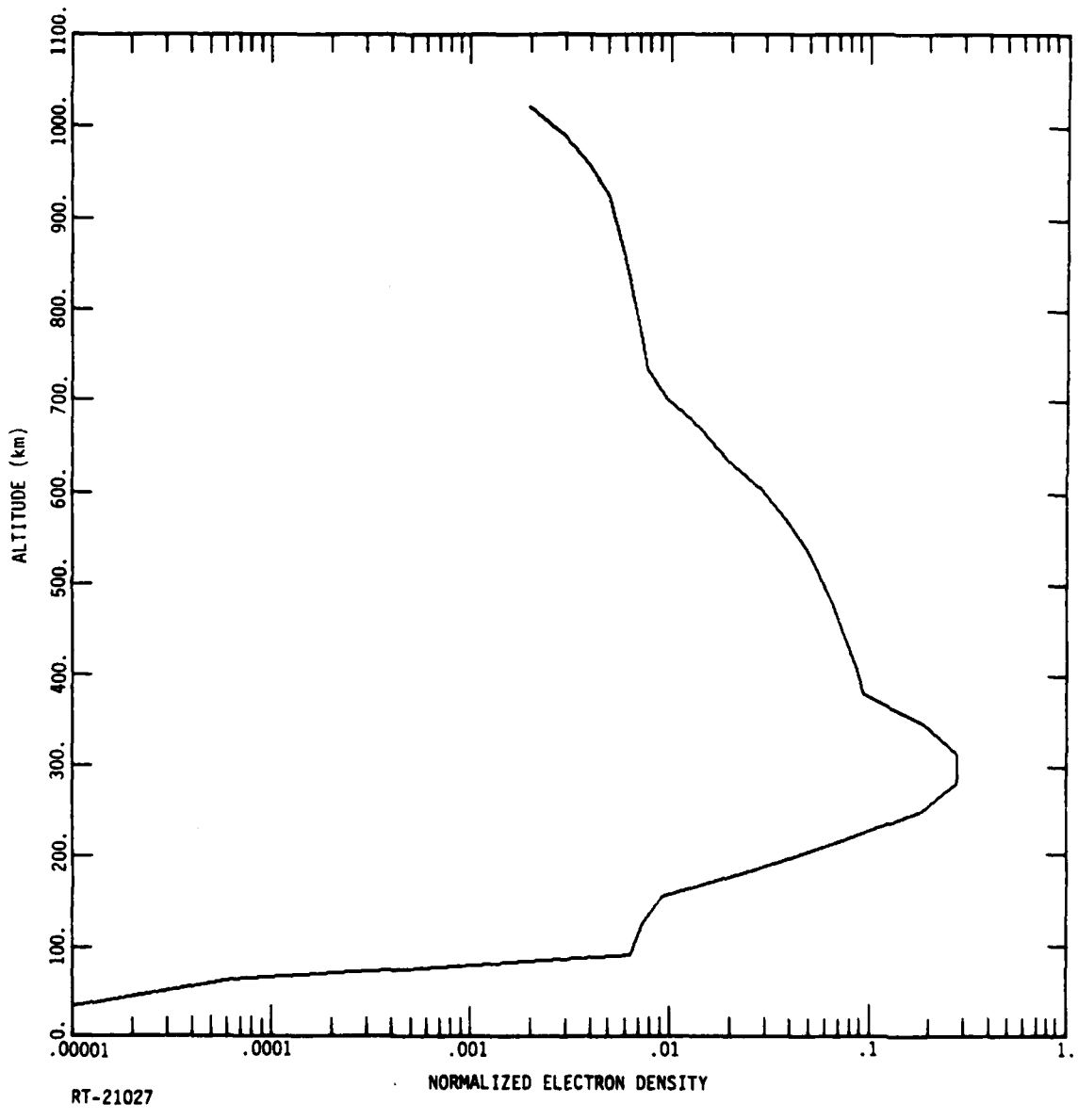

Figure 3. Reconstructed normalized electron density profile obtained with the time domain inverse scattering technique and a noise fraction of zero. Maximum deviation is 2.98×10^{-8} and RMS deviation is 1.08×10^{-8}.

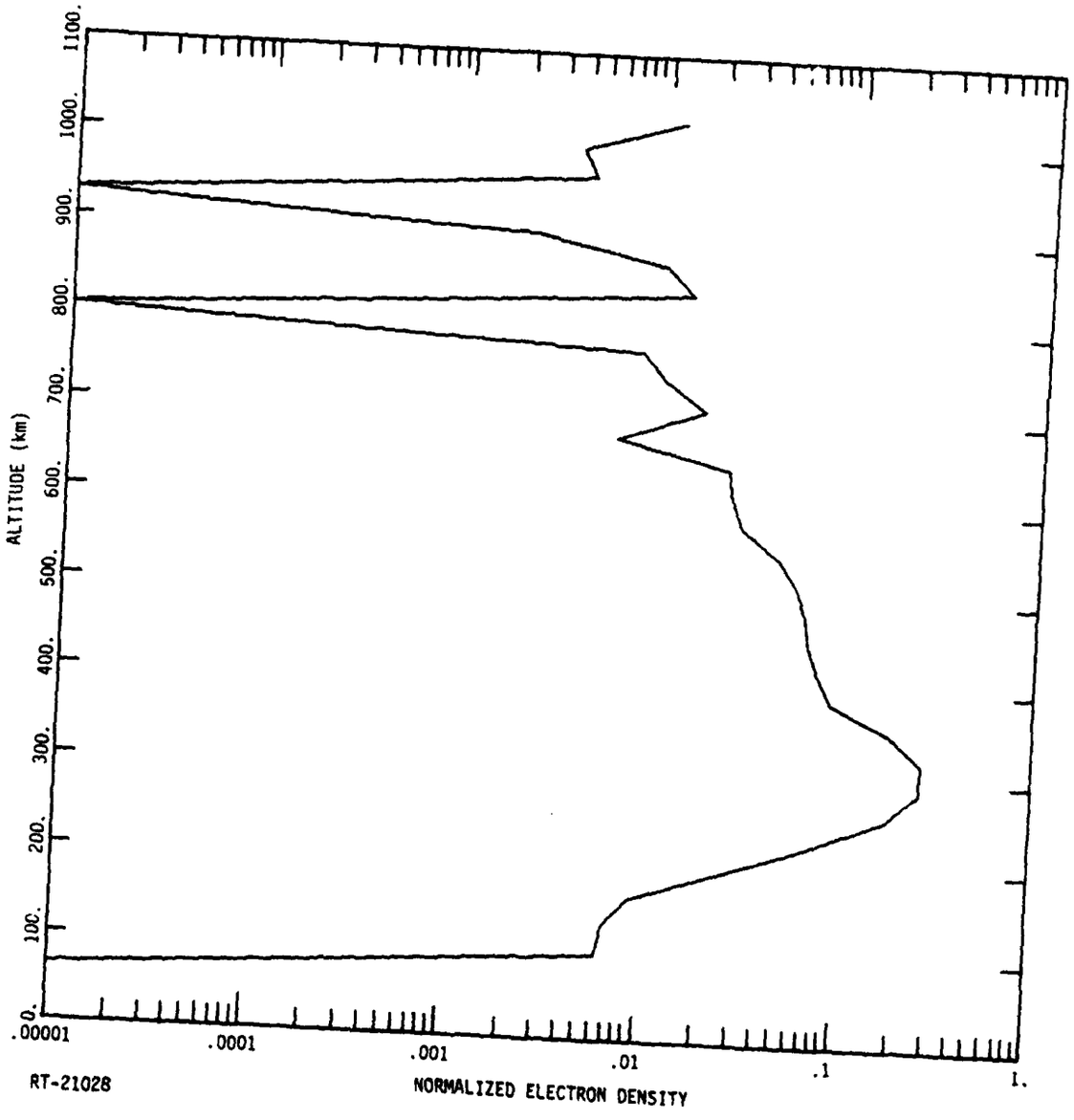

Figure 4. Reconstructed normalized electron density profile obtained with the time domain inverse scattering technique and a noise fraction of 1×10^{-2}. Maximum deviation is 1.07×10^{-2} and RMS deviation is 4.82×10^{-3}.

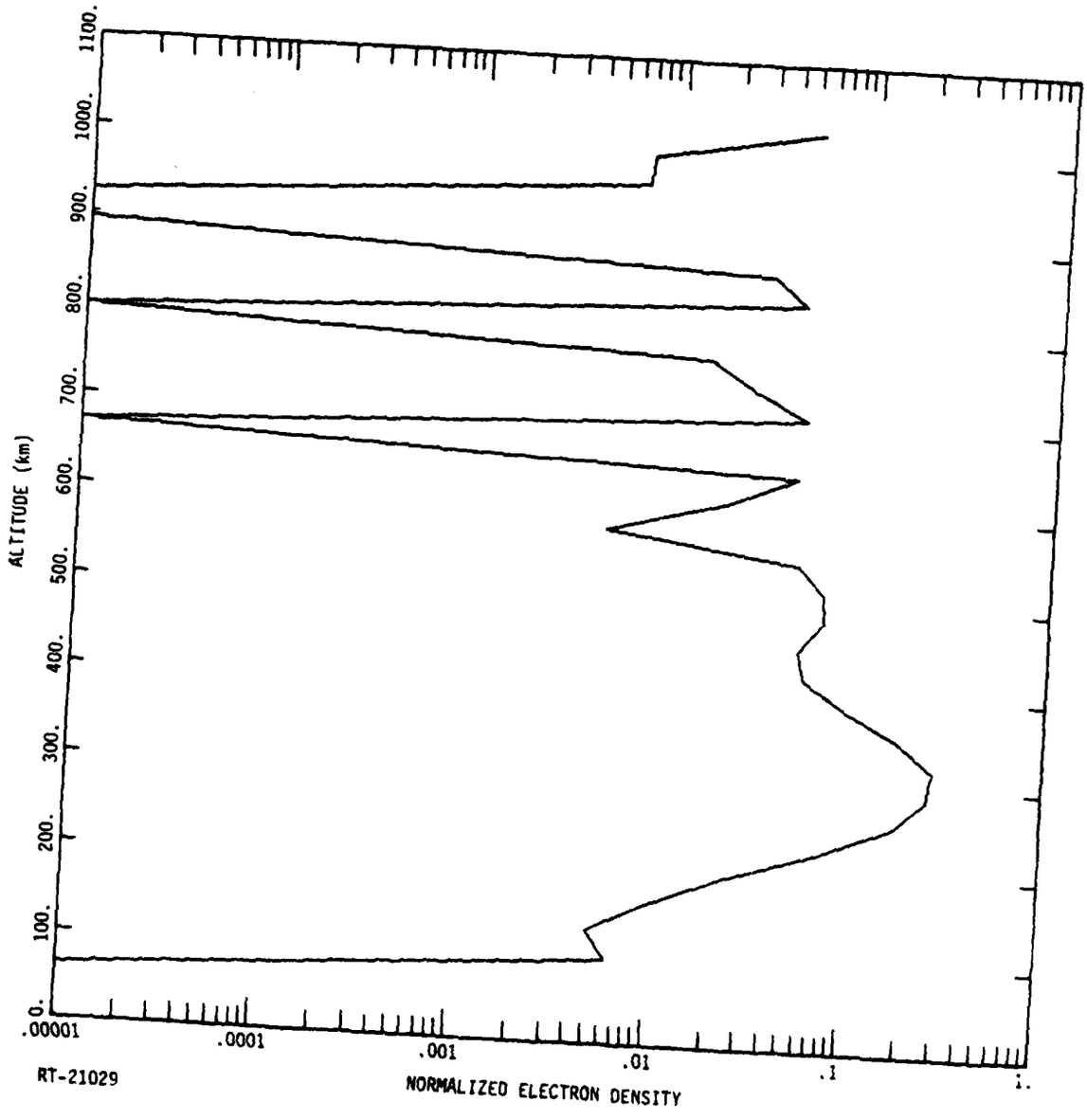

Figure 5. Reconstructed normalized electron density profile obtained with the time domain inverse scattering technique and a noise fraction of 5×10^{-2}. Maximum deviation is 5.17×10^{-2} and RMS deviation is 2.26×10^{-2}.

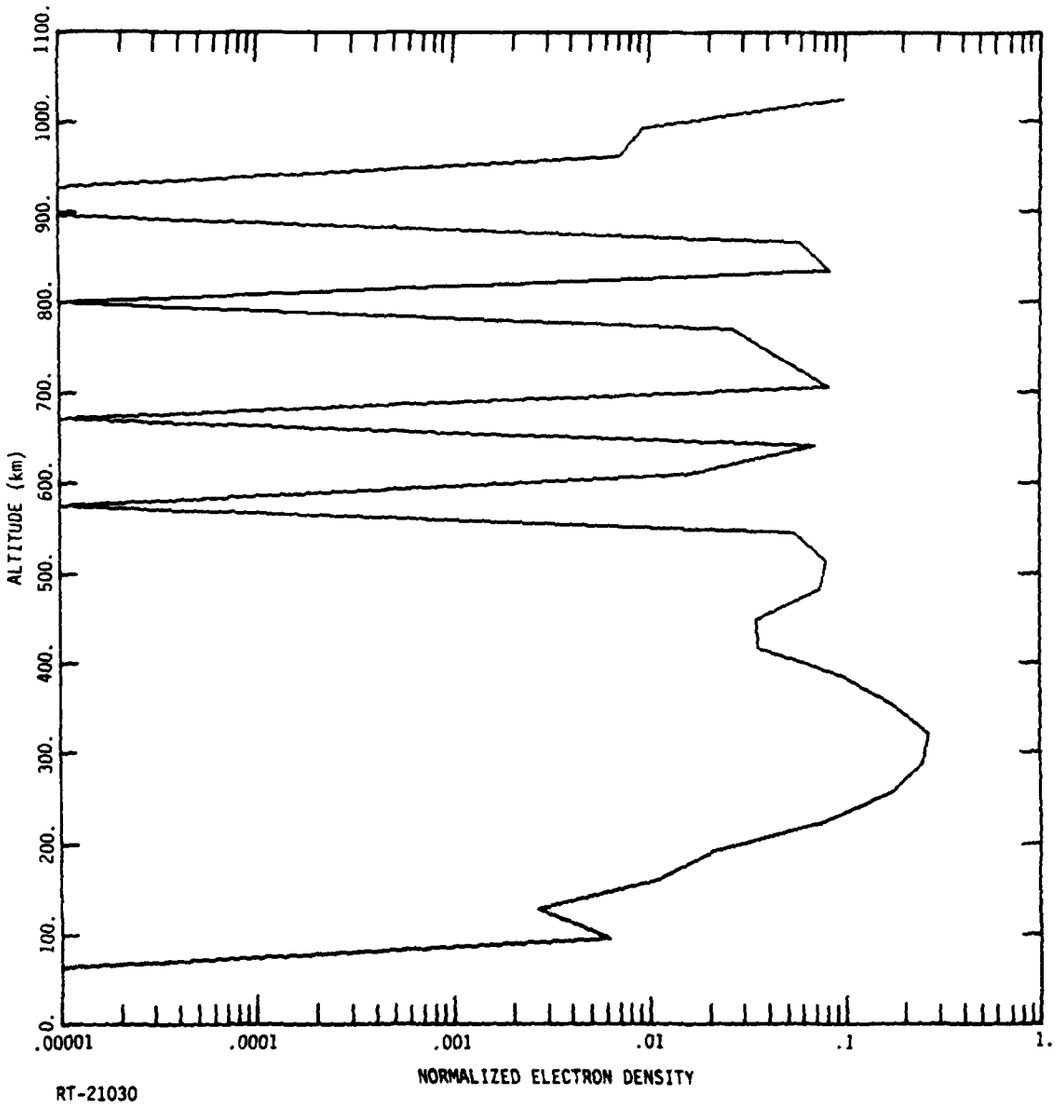

Figure 6. Reconstructed normalized electron density profile obtained with the time domain inverse scattering technique and a noise fraction of 1×10^{-1}. Maximum deviation is 9.75×10^{-2} and RMS deviation is 4.17×10^{-2}.

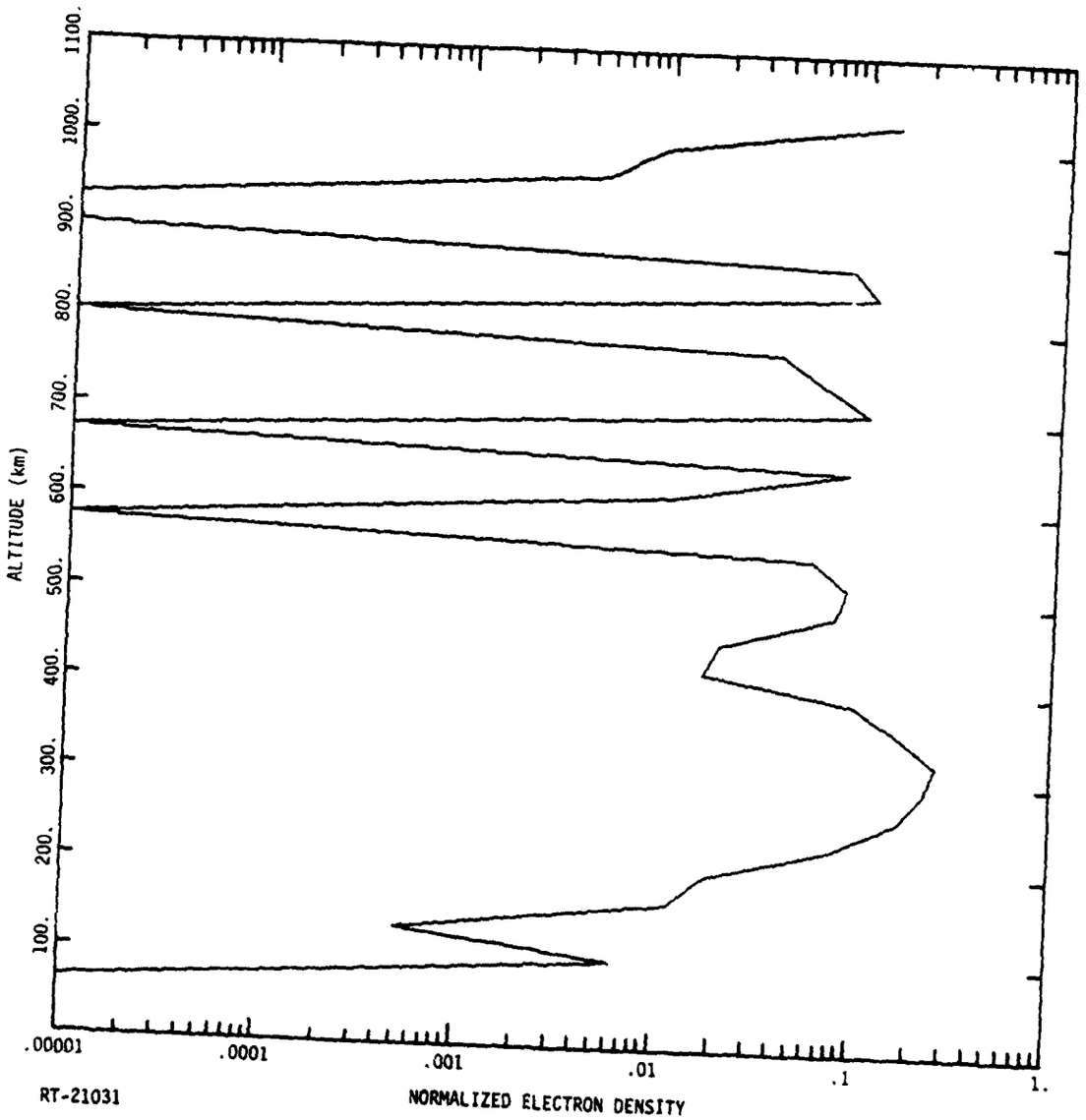

Figure 7. Reconstructed normalized electron density profile obtained with the time domain inverse scattering technique and a noise fraction of 1.5×10^{-1}. Maximum deviation is 1.36×10^{-1} and RMS deviation is 5.75×10^{-2}.

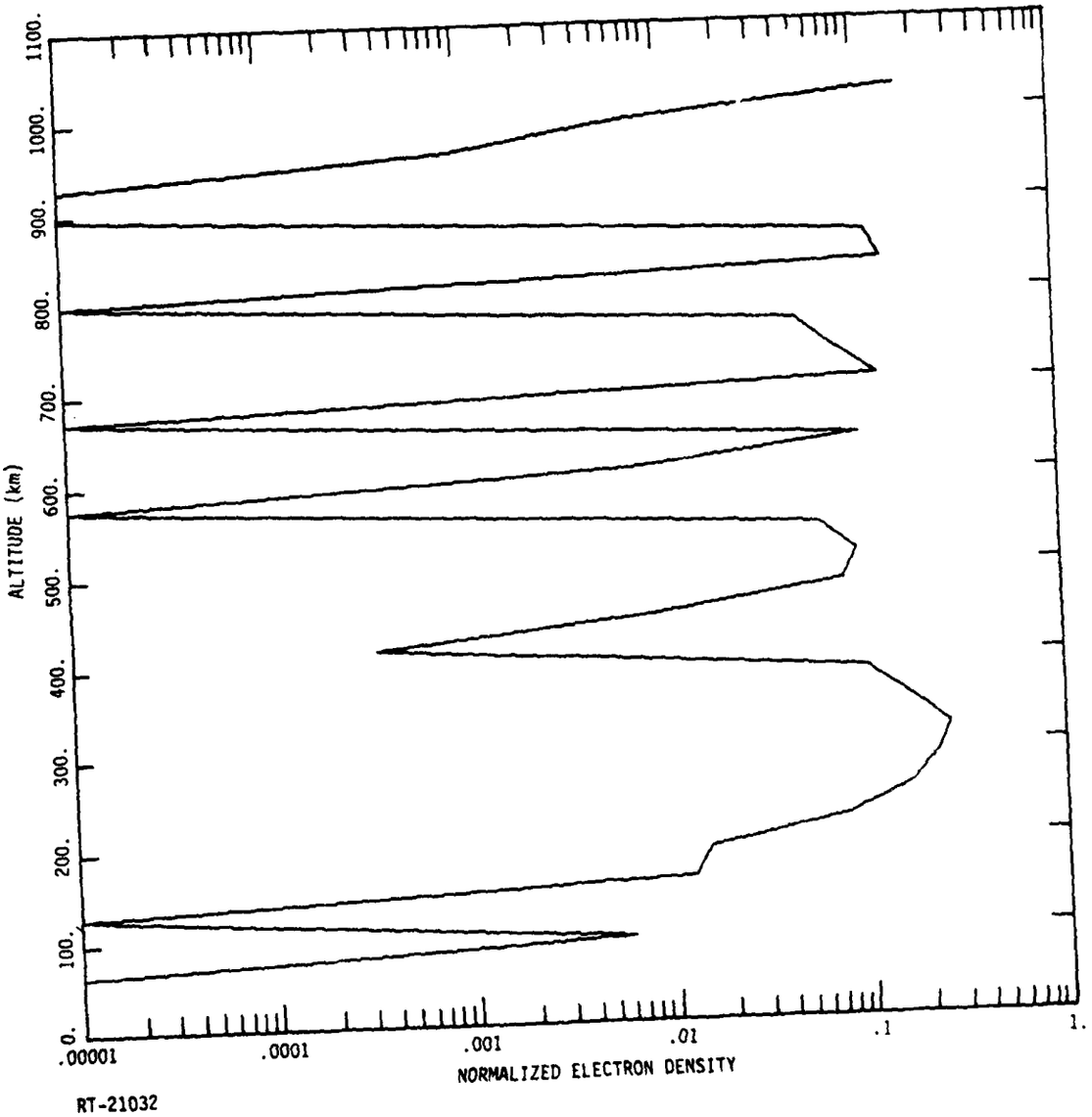

Figure 8. Reconstructed normalized electron density profile obtained with the time domain inverse scattering technique and a noise fraction of 2.0×10^{-1}. Maximum deviation is 1.67×10^{-1} and RMS deviation is 7.07×10^{-2}.

equal to $i\rho$. It is also shown that, for reconstructions of the ionosphere, the intensity of the holographic field is proportional to the electron density. It follows that the results from the author's Holographic Radio Camera demonstration experiment, summarized in Section 6, are, in fact, excellent examples of the type of reconstruction obtainable using inverse scattering techniques.

6. PRACTICAL ASPECTS OF USING INVERSE SCATTERING TO PROBE THE IONOSPHERE

This section considers several practical aspects of applying inverse scattering techniques to detemrine the three-dimensional electron density distribution of the ionosphere. The effects of noise in measurements are considered in Section 6.1. Section 6.2 examines the effects of incomplete, spatially sampled measurements, and the resolution which can be achieved. Since the results in these two subsections have been available previously, they are only summarized here. Section 6.3 examines the choice of probing frequency, and shows why scalar measurements may be sufficient with the proper choice of frequency. Section 6.4 presents the important result that, again with the proper choice of frequency, and with certain other conditions satisfied, it may not be necessary to carry out the full solution to the Exact Theory to obtain the relative distribution of electron density. Finally, Section 6.5 reviews the Holographic Radio Camera demonstration experiment as an example of how the type of data required for inverse scattering measurements can be taken, and what results were obtained using the simpler processing described in Section 6.4.

6.1 THE EFFECTS OF NOISE MEASUREMENTS

The effects of measurement noise on the reconstructed refractive index obtained using the theory of Section 2 can be seen by writing $\phi_H(\underline{x}) = \phi_H(\underline{x}), + \phi_N(\underline{x})$ where $\phi_N(\underline{x})$ contains a contribution due to noise. It follows, using Equation 12, that this is equivalent to a source term $\rho(\underline{x}) + \rho_N(\underline{x})$, where $\rho(\underline{x})$ is the true source and $\rho_N(\underline{x})$ contains the effect of the noise. From this it can be seen that the signal-to-noise ratio of the solution is the signal-to-noise ratio of $\phi_H(\underline{x})$. Since $\phi_H(\underline{x})$ depends on the integral over the measurement surface of the measured field values (Equation 4), the signal-to-noise ratio of $\phi_H(\underline{x})$ [and thus of $\rho(\underline{x})$] is not less than (and may be greater than) the signal-to-noise ratio of the measured data. This has been confirmed by numerical experiments (Ref 52). Recently, the author (Ref 78) has proven analytically that the signal-to-noise ratio of $\rho(\underline{x})$ is greater than or equal to the signal-to-noise ratio of the measured data.

6.2 THE EFFECTS OF INCOMPLETE MEASUREMENTS, AND RESOLUTION

Practical inverse scattering problem measurements almost always involve discrete measurements over a limited aperture, as opposed to the continuous measurements over a closed surface used in the above theory. Mager and Bleistein (Ref 79) have shown that, in the physical optics limit, the spatial bandwidth over which measured data is known is the spatial bandwidth over which the source term can be determined. A similar but more general result follows directly from analysis of the three-dimensional spatial Fourier transform of Equations 4 and 12. Let $\underline{\nu}$ be the spatial frequency variable, and let capital letters denote the transformed functions. For the general case, $\Phi_H(\underline{\nu})$ is known over the whole surface S, and thus for all $0 \leq \underline{\nu} \leq \underline{\nu}_o$ (the upper bound is $\underline{\nu}_o$ rather than ∞, since D, and thus S, are of finite size). Since the left side of the transformed version of Equation 12 is known for all $0 \leq \underline{\nu} \leq \underline{\nu}_o$, it follows that $P(\underline{\nu})$ is determined over this range. Now let $\phi(\underline{x})$ be measured at discrete points over a limited aperture. Then $\Phi(\underline{\nu})$ is determined for $\underline{\nu}_1 \leq \underline{\nu} \leq \underline{\nu}_2$, where these spatial bandlimits are determined by the aperture size and sample spacing. It follows from the transform of Equation 4 that $\Phi_H(\underline{\nu})$ is similarly bandlimited, and from the transform of Equation 12 that $P(\underline{\nu})$ can be determined over this band of spatial frequencies.

A related but more general result on the resolution obtainable in a coherent imaging process has been obtained by the author (Ref 80). The lateral resolution for a coherent process is $\Delta x = (\lambda z/D)(\Delta\phi/2\pi)$, where λ is the wavelength, z is the distance from the aperture to the target, and D is the size of the aperture over which the data is recorded. $\Delta\phi$ is the accuracy with which phase can be measured across the aperture. Note that as $\Delta\phi \rightarrow 2\pi$, the resolution goes to the classical (Rayleigh) result for incoherent imaging. The second term, involving $\Delta\phi$, represents the gain in resolution as a result of the added information present in the phase recorded in a coherent process. A similar result is obtained for the longitudinal resolution: $\Delta z = (\lambda z^2/D)(\Delta\phi/2\pi)$. The accuracy with which phase can be measured is determined by the power signal-to-noise ratio of the measurement, S/N: $\Delta\phi = (2S/N)^{-1/2}$. These theoretical results have been verified by numerical experiments (Refs 13,52,80) and by results obtained with the Holographic Radio Camera (see Section 6.5).

6.3 THE CHOICE OF PROBING FREQUENCY: WHEN ONLY SCALAR MEASUREMENTS ARE NEEDED

Section 2.4 derived the equations for, and discussed the solution to, the Exact Inverse Scattering Theory for vector fields and anisotropic media. Sections 1.2 and 2.3 discussed the equations applicable to the description of such media. The complications introduced by anisotropic media and the need to measure and process vector field data are significant. It would be very important if conditions under which scalar field measurements and scalar processing could yield electron density distributions could be identified. Fortunately, this is the case.

Consider Equations 13 and 14 for the refractive index, n, of a magneto-ionic medium. Assume that the region of interest in the ionosphere is above ~ 70 km altitude. Now consider the relative magnitudes of the four terms (Equation 14) which contribute to n. Above ~ 70 km, the maximum collision frequency, ν, is $\leq 5 \times 10^5$ Hz (c.f. Ref 2, Table 1.3). At a probing frequency of $\geqslant 100$ MHz, $Z \leq 8 \times 10^{-4}$. This is negligible compared to the 1 in the denominator of Equation 13, and n can be treated as real. The earth's magnetic field has a magnitude of $\sim 5 \times 10^{-5}$ web/m^2. Thus eB/m$\leqslant 8.8 \times 10^6$, and Y_L and Y_T are $\leq \sim 10^{-2}$ at frequencies above 100 MHz. It follows that terms of order Y^2 can be neglected with respect to 1 in the denominator of Equation 13. The result is that, for frequencies above ~ 100 MHz, the refractive index is given by Equation 15. This is independent of the direction of propagation with respect to the magnetic field, and the ionosphere behaves isotropically. At such frequencies, scalar measurements and scalar processing are sufficient.

A frequency of 100 MHz or higher is preferred for at least two other reasons. At HF (3-30 MHz) frequencies and below, significant reflection occurs in the ionosphere. Within the context of inverse scattering, this means that the backscattered component becomes significant, and reconstructions using measurements primarily sensitive to the forward scattered component (e.g., ground-based measurements with a satellite-borne source) would suffer a loss of sensitivity. Also, structure of interest may have scale sizes of the order of from several tens of meters to 100 meters. As discussed in Section 6.4, it is often desirable to have the wavelength be small compared to the structure.

6.4 THE RELATIONSHIP BETWEEN HOLOGRAPHY AND INVERSE SCATTERING

It was noted in Section 2.1 that the quantity in which the field measurements appear, ϕ_H (Equation 4), is the field obtained by reconstructing a hologram recorded

over the measurement surface. It is therefore to be expected that there would be a close relationship between holography and inverse scattering. Indeed, this is the case, and a very important approximation comes out of this relationship.

Optical holographers often seek to probe an inhomogeneous medium by obtaining images at various depths. Indeed, humans solve an inverse scattering problem every time they recognize an object from its image. Imaging is an inverse scattering problem: Based on observed field data, information about the scatterer (contained in $\rho(\underline{x})$ in the formulation of Section 2.1) is sought. If only the shape of the scatterer is sought, then it can be shown that a physical optics far-field approximation to the exact inverse scattering solution is often sufficient (Refs 11,81). However, if any information other than the shape is desired (e.g., the complex refractive index), then the full exact solution is required.

It was noted above that ϕ_H is the field obtained from a holographic reconstruction. From Equation 9 ,

$$\phi_H = \phi - \int dV\, g^* \rho \tag{51}$$

Several conclusions follow from this equation:

1. ϕ_H is a field. It is not the source term, ρ. The source term, ρ, contains <u>all</u> the information about the source. Simple examination of the holographic reconstruction, ϕ_H, cannot in general give ρ. To obtain ρ, Equation 12 must be solved.

2. Holographers commonly make the statement, "The holographic reconstruction is the field which existed in object [source] space." This is an approximation which, from Equation 51, is given by

$$\phi_H \approx \phi \tag{52}$$

3. If, and only if, the scatterer is of such a form, and if, and only if, the wavelength and all other dimensions in the problem are such that the field scattered by the scatterer has a perturbation introduced into it which is the shape of the scatterer, then, to the degree that Equation 52 holds, it is possible to deduce the shape of the scatterer from a holographic

reconstruction. In other words, the shape can be deduced when the field "looks like" the scatterer. This is often true for objects with sharp edges imaged using optical holography.

4. The approximation of Equation 52 can only be true when the second term of Equation 51 is 0. The kernel, g^*, is of the form $\left[\cos(kr) - i \sin(kr)\right]/4\pi r$. The integral will thus be small as $r \to \infty$. Thus, the statements of paragraphs 2 and 3 hold only in the far field. Note that this requires that reconstructions, "near" enough the position of the scatterer so that the feld "looks like" the scatterer, must still be in the far field in terms of wavelengths.

The statement, that the requirement that the scattered field "look like" the scatterers, is often true for objects with edges that are "sharp" and can be expressed in a more quantitative manner. Consider the kernel of the integral in Equation 12. In three dimensions, Img is given by

$$\text{Img} = \sin(kr)/4\pi r \tag{53}$$

Using convolution notation, Equation 12 can be written as

$$\phi_H = 2i\,\rho * \sin(kr)/4\pi r \tag{54}$$

Now consider the short wavelength limit. As $\lambda \to 0$, $\sin(kr)/4\pi r \to \delta(r)/2$ (where δ denotes a three-dimensional delta distribution), and

$$\lim_{\lambda \to 0} \phi_H = 2i\,\rho * \delta(r)/2 \tag{55}$$

$$\lim_{\lambda \to 0} \phi_H = i\rho \tag{56}$$

Physically, this says that when the wavelength is small enough compared to any structure in the scatterer (i.e., the edges of the scatterer are "sharp"), the convolution with Img acts like a convolution with a delta distribution, replicating the scatterer in the field ϕ_H.

Equation 56 is a very important result for ionospheric probing. Consider the use of frequencies above 100 MHz, and restrict interest to spatial resolution large compared to the wavelength. Then Equation 56 is a good approximation, and Equation 15

for the refractive index also applies. From Equation 3 it can be seen that $\rho(\underline{x})$ is proportional to $n^2(\underline{x})-1$, which in turn, from Equa' · 15, is proportional to $N(\underline{x})$, the desired spatial distribution of electron de ,. Suppose that the quantity $(\phi_H(\underline{x})\phi_H(\underline{x})^{\frac{1}{2}}$--the magnitude of the reconstructed holographic field--is computed. From Equation 56 this will be proportional to $\rho(\underline{x})$ and thus to $N(\underline{x})$. Providing the short wavelength limit is satisfied, the magnitude of the reconstructed holographic field is proportional to the electron density distribution.

One of the major reasons this is such a powerful result is the accuracy and efficiency with which $\phi_H(\underline{x})$ can be computed, even in the presence of noise. Let $\mathcal{F}$ and $\mathcal{F}^{-1}$ denote spatial Fourier direct and inverse transforms, respectively, computed using FFT techniques. Then it can be easily shown (Ref 82, Sections 3-7; Ref 83, Section 5.4 and Appendix I) that:

$$\phi_H(x,y,z) = \mathcal{F}^{-1}\left\{\mathcal{F}\left\{\phi(x,y,0)\right\}\exp\left\{ikz\left[1-(\lambda\nu_x)^2-(\lambda\nu_y)^2\right]^{\frac{1}{2}}\right\}\right\} \tag{57}$$

In Equation 57, $\phi(x,y,0)$ is the data recorded on the ground, ν_x and ν_y are spatial frequency variables, and the Fourier transform operations are two dimensional, from (x,y) space to (ν_x,ν_y) space. Equation 57 is derived from Equation 4 by noting that the integral in Equation 4 involves two-dimensional spatial convolutions, applying the convolution theorem of Fourier analysis, and analytically evaluating the two-dimensional spatial Fourier transform of g^*. Direct evaluation of Equation 4 using numerical integration would require sampling the integrand at intervals small compared to the periods of its oscillation. These periods are of the order of λ/d, where d is any dimension of interest. This is clearly impossible from either a measurement or a computation standpoint. Equation 57 totally avoids this problem, and is more efficient and accurate as well.

6.5 THE HOLOGRAPIC RADIO CAMERA

The previous subsection explained the close relationship between holography and inverse scattering. The Holographic Radio Camera demonstration experiment (Refs 4,5) was carried out to provide a visualization of ionospheric structure: Images of the electronic density distribution. A summary of the experiment, its results, and the important insight about ionospheric structure obtained from these results is given in this subsection. This material is included in this paper because it is an example of how the data used in inverse scattering can be recorded, and an excellent demonstration of

the practicality of such measurements. In particular, it demonstrates how images of the ionospheric electron density distribution can be obtained using the simplified inverse scattering techniques of the previous subsection.

Historically, the ionosphere has been viewed as having a structure dominated by random turbulence. The primary basis for this picture has been ground-based observations of the temporal spectra of the fluctuations, or scintillations, introduced on signals from satellites or stellar radio sources. Because of the lateral motion of the ionosphere with respect to the source, these temporal spectra can be interpreted in terms of the spatial frequency spectrum of the irregularity structure in the medium. These spectra display a power-law dependence of power spectral density on spatial frequency. Because this is consistent with the spectra which would be observed if the ionosphere had a turbulence-dominated structure, such a structure has been inferred. The results thus far from the Holographic Radio Camera suggest that a far more orderly structure may, in fact, be the case, at least for the mid-latitude ionosphere.

Holography is the process of recording, coherently, the amplitude and phase of a wave. The Holographic Radio Camera accomplishes this at a ~ m wavelength. In the demonstration experiment described here, 32 antennas, separated 32 m apart, were laid out along an east-west line (near La Posta, California, at a latitude of $\sim 32^{o}$N). The same local oscillator signal was distributed coherently along this 1 km line array, and the intermediate frequency signals were sampled, digitized, and recorded such that the phase and amplitude of the field at each antenna was recorded coherently as a function of time. The radio sources for the experiment were the Navy Navigation Satellite System (NNSS) satellites, which are in circular polar orbits at an altitude of 1000 km. For orbits on which the satellite was at a high enough elevation angle to be in the main lobe of the vertically pointing antennas, the motion of the satellite, during the portion of the pass when it was directly overhead, was approximately perpendicular to the line of the array. By sampling in time, aperture synthesis occurred and a series of ~1 km by ~1 km radio frequency holograms, each consisting of 32 x 32 points, was obtained. The details of the sampling and recording, and an in-depth analysis of the aperture synthesis approximation and of the resulting corrections applied to the data are given in Reference 4.

The resulting holograms were processed by a computer to obtain reconstructions of the ionosphere at a series of altitudes between 200 km and 600 km. Mathematically, the reconstruction process involved evaluating Equation 57. Because of the choice of

wavelength and the resolution and the geometry of the measurements, the field magnitudes presented below can be considered to be proportional to the electdron density distribution at the altitude of reconstruction (see Section 6.4).

6.5.1 Experimental Results

Figures 9 through 12 show examples of the reconstructions obtained to date with the Radio Camera. The data for these figures were taken on July 24, 1976, at approximately 5:19 a.m. local time. The satellite passed over the array within three degrees of the north-south line. The two end antennas were recorded as having zero signal due to cable problems. The data frames used to produce these figures were taken over approximately a 30 second time span centered about the zenith time (5:19 a.m.). Vertical incidence ionograms recorded adjacent to the array, five minutes before and after the zenith time, indicate that the ionosphere was "quiet" and relatively unchanging, with some slight sporadic E present.

The field magnitude reconstructed at an altitude of 300 km is shown in Figure 9. The east-west and north-south directions are as indicated and this orientation of the reconstructions is used in all the figures. The sampling interval is 32 m east-west, and approximately 24.5 m north-south. Figure 10 shows a number of reconstructions of the field magnitude from a single frame of data, at the indicated altitudes. The 0 km diagram represents the magnitude of the field recorded on the ground by Radio Camera. The striking feature present in both figures is the highly periodic structure, present in both directions. At 300 km altitude, the period of the structure is about 800 m north-south and about 300 m east-west. As shown in Figure 10, the periods in both directions remain approximately constant over the range of altitudes from 300 to 500 m. There is significantly more fine-period structure present at the 200 m altitude than for higher altitudes.

Figure 11 shows the reconstructions of the phase of the field which correspond to the magnitude data in Figure 10. The dimensions are the same for both sets of reconstructions. The "vertical" axis on each reconstruction is the same, representing a maximum phase excursion from $-\pi$ to π radians. In order to permit the structure to be seen from a single viewing direction in the isometric, hidden line display, noise peaks in the phase reconstructions have been zeroed (this is done for display purposes only). Note that the same type of periodocity present in the magnitude is seen in the phase. However, there is a noticeable decrease in the magnitude of the phase excursions near the altitude of 400 km.

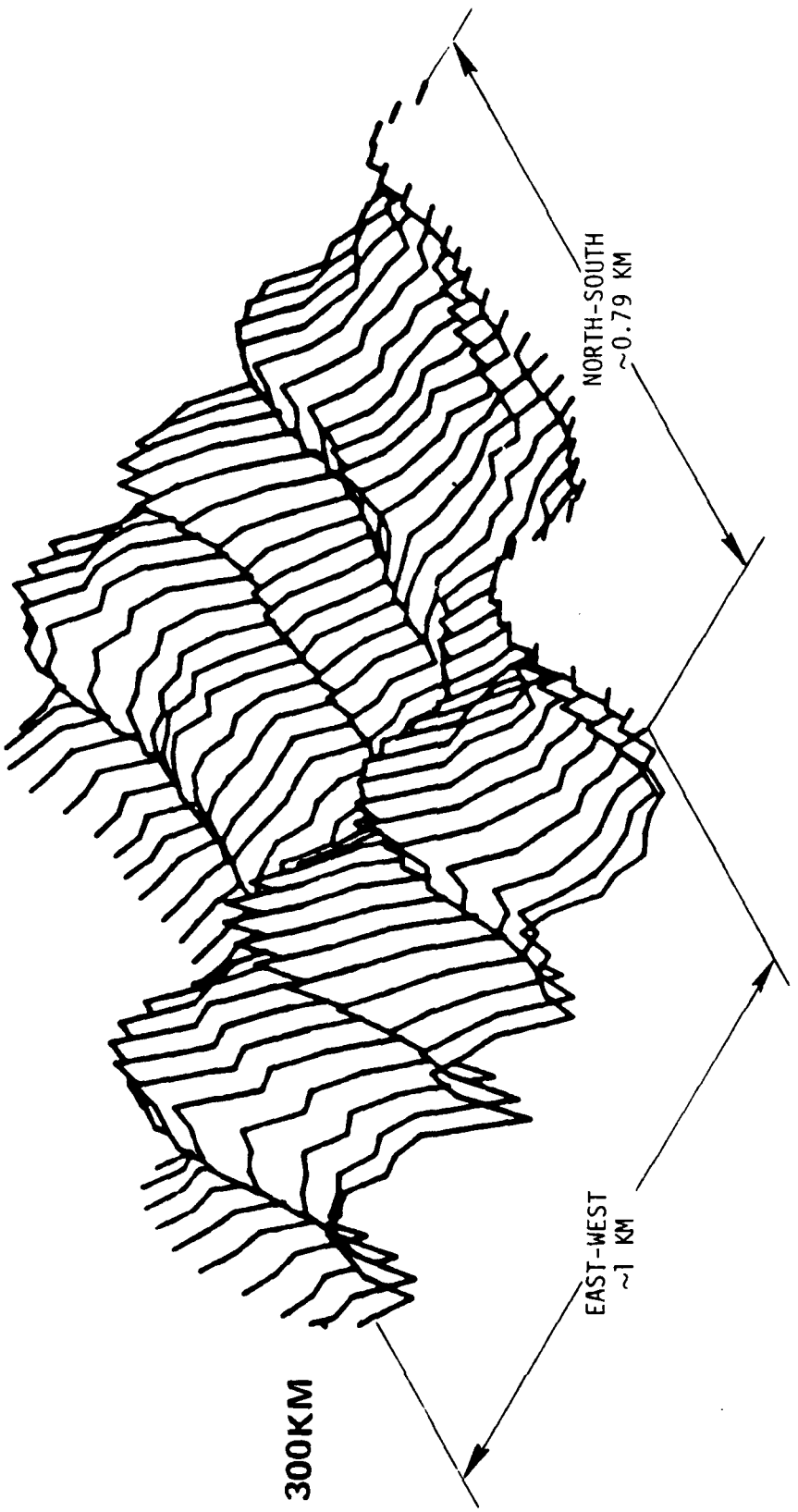

Figure 9. Magnitude of the field reconstructed at an altitude of 300 km

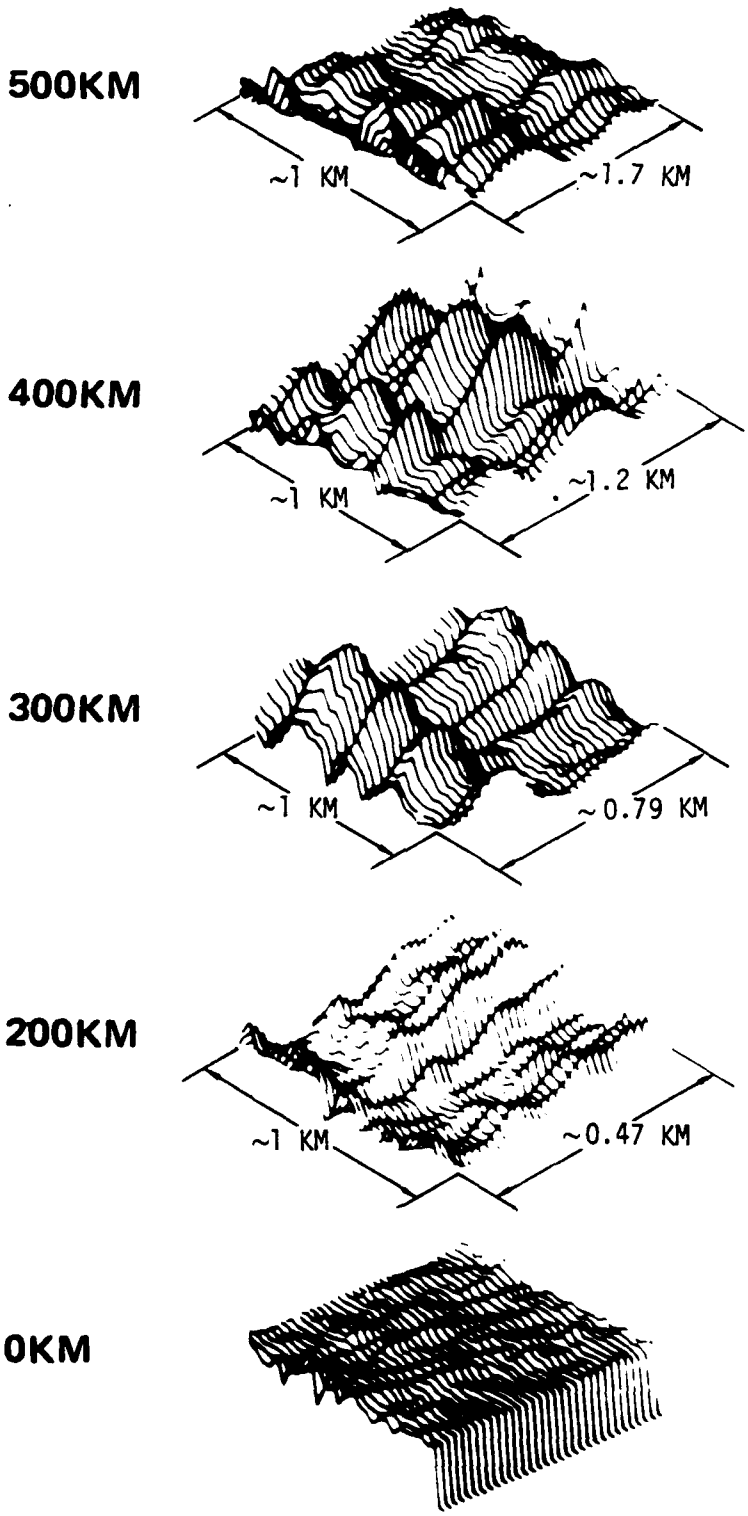

Figure 10. Reconstructions of the magnitude of the field at the indicated altitudes. The effective dimensions of the array in each direction are shown for each altitude.

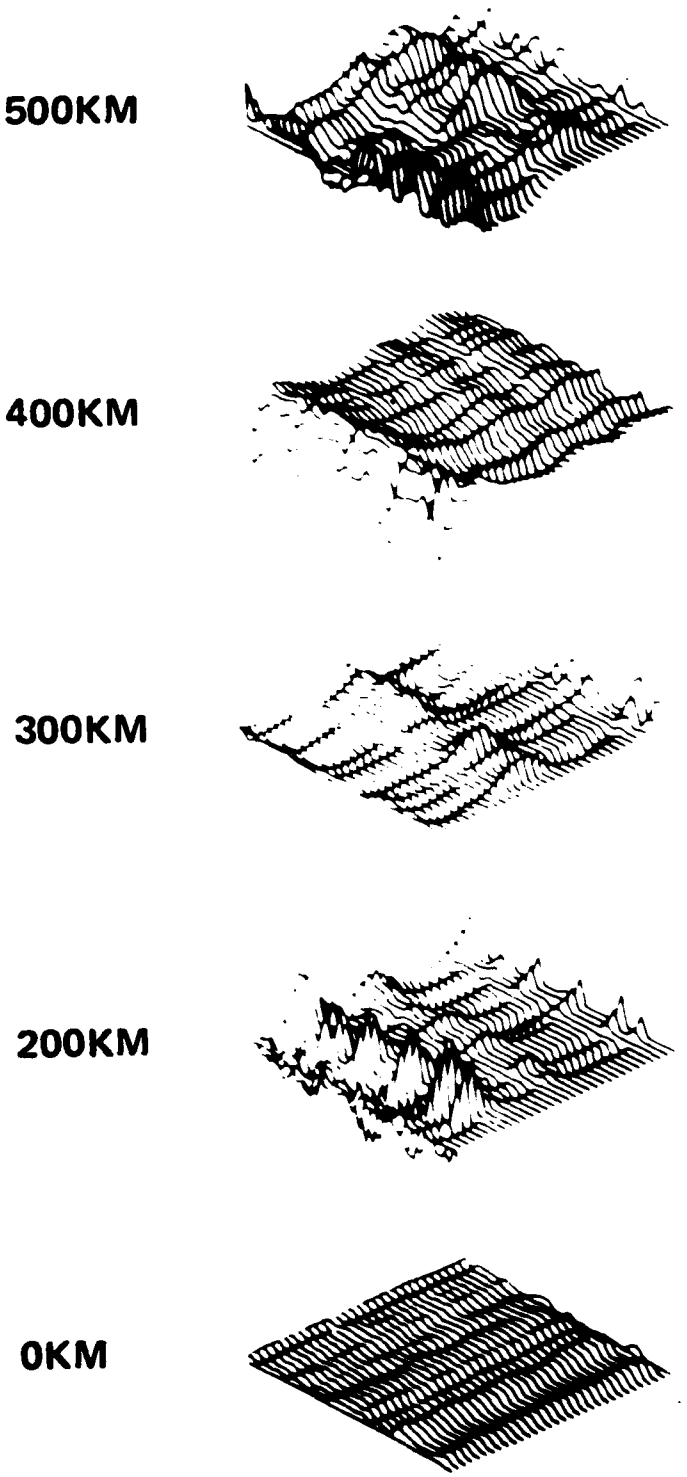

Figure 11. Reconstructions of the phase of the field at the indicated altitudes

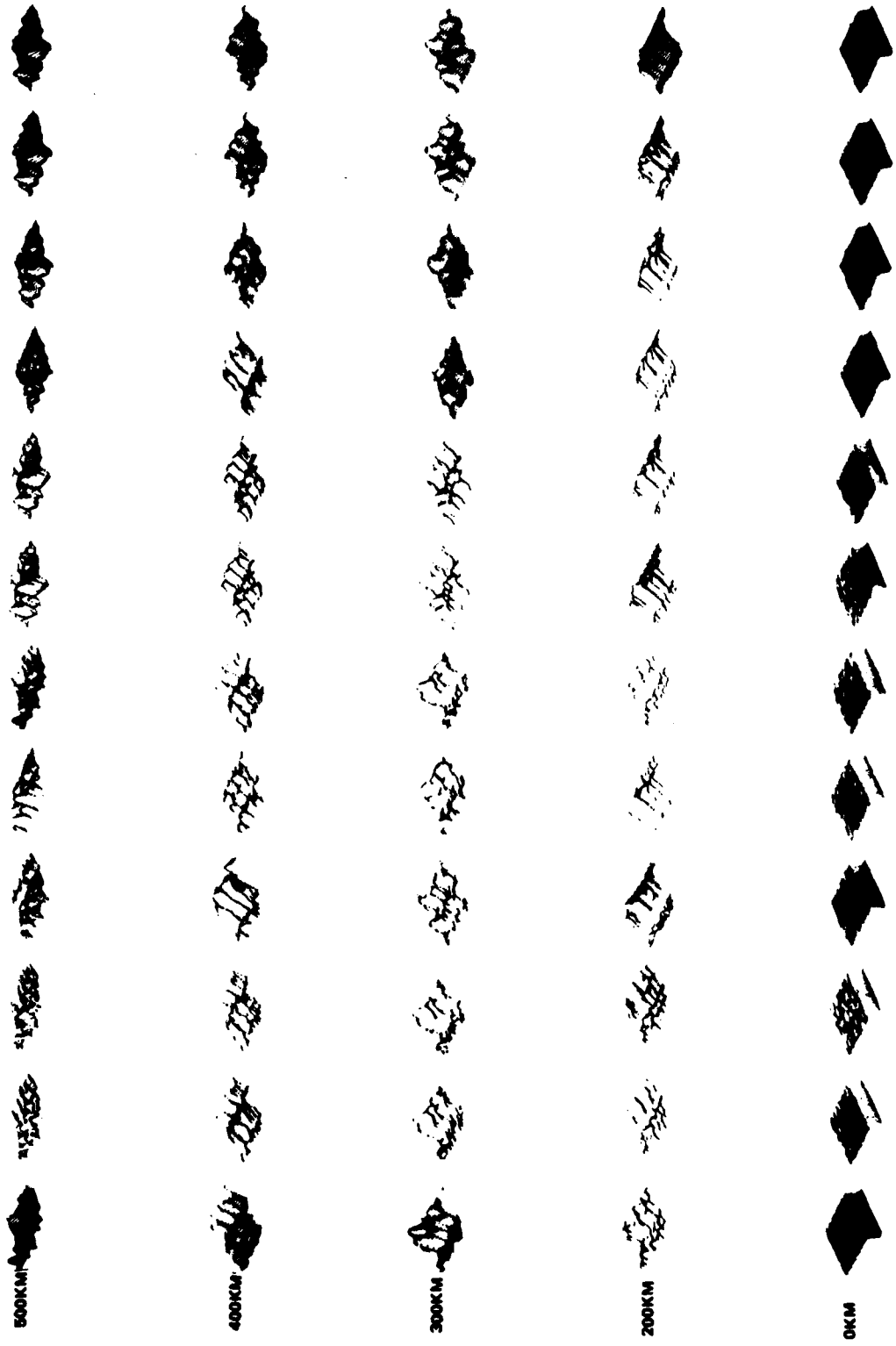

Figure 12. Reconstructions of the field magnitude at the indicated altitudes for successive frames of data. The spacing between frames at a given altitude is approximately 6.25 times the north-south dimension of the reconstruction at that altitude, as shown in Figure 9. The data for these reconstructions were recorded on July 24, 1976 at 5:19 a.m. local time.

The method of visually displaying the data actually used in the laboratory permits the reconstruction to be oriented at an arbitrary angle in three-space with respect to the viewer, and with either isometric or full perspective display. Considerable information is lost by fixing the orientation and reducing the plots for publication. As a result, some of the geometrical aspects mentioned in this section may appear to be less convincing in the printed figures than they are in the laboratory.

Figure 12 presents magnitude reconstructions from twelve frames of data. The satellite was at zenith between the sixth and seventh frames from the left. Note that there is a significant amount of uniformity in the periodicity of the structure at a given altitude in each direction. Furthermore, the period of the structure in each direction is approximately the same at 300, 400, and 500 km altitude for many frames. Much finer structure is observed at 200 km in both directions.

Observations on several other days, at different local times, produced similar (although by no means identical) results.

6.5.2 Interpretation

For the ionosphere, significant levels of electron density often exist at all altitudes between ~80 km and the altitude of the satellite. However, it is precisely an assumption of free space propagation upon which the concept of modeling the ionosphere as a "thin screen" is based [Booker, Ratcliffe, and Shinn (Ref 84); Rufenach (Ref 85); Bramley (Ref 86)]. In this model the fluctuations imposed on the radio wave due to passage through the ionosphere are confined to a thin layer (typically assigned an altitude in the range from 200 to 400 km). Immediately below this layer the fluctuations are only in the phase of the wave. As the wave propagates through free space to the ground, amplitude fluctuations develop. Thus, the reconstructions of the field at a given altitude as presented above represent the field which would have to be postulated to exist just below a screen at that altitude to produce the observed field on the ground. Note that in order for the screen to be a phase screen, the reconstructed field should have essentially uniform amplitude: $\Delta A/A$ should be small compared to $\Delta \phi$ (where A is the amplitude and ϕ is the phase). If this were the case, the plot of the magnitude of the field would appear as a smooth plane at the altitude of the screen, while the phase plot would show significant fluctuations. None of the frames of data shown above or obtained with the Radio Camera display this property at the altitudes shown, between 200 and 500 km. The conclusion is that this experimental data cannot be explained in terms of a thin phase screen within this altitude range.

The reconstructions obtained to date have a single, visually striking feature in common--the predominate periodic structure. Although the currently available sample of processed reconstructions is too small to support firm conclusions about the mechanism producing this structure, it is interesting to speculate on the possibility that waves in the ionospheric medium could be this mechanism. The primary semi-quantitative observable involved is the apparent wavelength. However, the spaces between frames of data in the north-south direction and the resolution limiations prevent accurate determination of the wavelength, and make determination of the horizontal distance over which the periodic structure extends uncertain. Until additional data is available, interpretation of the results will be limited to consideration of whether structure such as that present in the reconstructions is consistent with the results of other experiments.

Current practice is to model the ionospheric plasma as a largely random, turbulent medium. The experiments to date upon which the most common pictures of ionospheric structure are based use, almost without exception, measurements integrated along the line of sight from the satellite to the ground (e.g., scintillation measurements). The most common analysis techniques applied to such measurements involve studies of the signal statistics, making an instantaneous description of the structure underlying a measured signal difficult. Spaced receiver measurements and analyses of the spectra of scintillations do permit the irregularity size to be determined. The dominant range of irregularity sizes reported for such measurements, at mid-latitudes, is from ~100 m to 1 to 2 km (this upper bound is probably due only to measurement limitations). These scales are of the order of the spatial periods present in the Radio Camera reconstructions.

However, it is not immediately obvious that these Radio Camera results are consistent with the fluctuation power spectra typically recorded in VHF scintillation experiments in mid-latitudes. The power spectra from individual frames of the Radio Camera data show peaks corresponding to the spatial periods present in the reconstructions. Typical results from the VHF scintillation measurements of other authors involve measurements over periods of time long compared to the time in which a frame of Radio Camera data was recorded. These results from other experiments show an inverse power law spectrum of irregularities which has been used to infer the turbulent medium model. When spectra from several successive frames of Radio Camera observations are averaged, similar inverse power law spectra are also obtained. This suggests that the difference between the two types of spectra might, in large measure,

be due to differences in the experiments in which they were recorded. The Radio Camera provides an instantaneous "snapshot" of the diffraction pattern, whereas the other techniques involve a lot of averaging. It seems possible that the Radio Camera is revealing a process of nonlinear interaction between different Fourier components of the plasma, which interaction in the long run leads statistically to an inverse power law spectrum of plasma turbulence. In other words, what has heretofore been described only as turbulence may, in fact, have an underlying wave-like structure. When the effects of propagation through this structure are averaged both spatially and temporally, the structure appears turbulent. Indeed, Booker (Refs 87,88) has put forth a consistent model of a whole range of ionospheric-radio wave interactions in which the underlying mechanism is nonlinear coupling of acoustic gravity wave energy (generated in the neutral atmosphere) into a spectrum of plasma waves.

7. CONCLUSIONS AND RECOMMENDATIONS

7.1 CONCLUSIONS

The following conclusions are drawn from this research. The conclusions listed are those that are new, based on the research reported in this paper. Conclusions available from review material included in this paper are not listed. These conclusions are listed in their order of presentation in previous sections.

1. The Exact Inverse Scattering Theory is the best available technique for determining the three-dimensional electron density distribution of the ionosphere, using measurements of the scattering of electromagnetic waves entering the ionosphere from outside the earth's atmosphere.
2. The Exact Inverse Scattering Theory for vector fields has been presented. It has been shown how, within the context of the magneto-ionic theory, measured vector field data can be used to obtain the three-dimensional distribution of both electron density and collison frequency in the presence of the earth's magnetic field.
3. A method of processing vector field data using the scalar equations of the Exact Theory to obtain the electron density and collision frequency distributions was obtained.
4. The uniqueness of the solution to the inverse scattering problem has been proven for the vector electromagnetic field case.
5. Three additional proofs have been presented, substantiating the previous proof by the author that nonradiating sources of compact support are physically inconsistent with Maxwell's equations, and thus do not exist.
6. An expression for the fundamental quantity, in Bojarski's exact, closed-form, analytic solution for the total field in the inverse scattering problem, in terms only of Fourier transform operations on the measured fields was presented.

7. An exact, closed-form, analytic solution for the source term in the inverse scattering problem has been obtained.

8. The numerical solution to the exact inverse scattering integral equation was implemented and studied for the two-dimensional case. Several preliminary results related to this numerical solution and to deconvolution problems in general were obtained, as given in Section 5.1.

9. It was shown that analytic solutions of the type associated with many solutions to the wave equation in terms of special functions, for analytic refractive index profiles (e.g., the Epstein profile), are not applicable to modeling forward scattering ionospheric experiments of the type considered in this paper. This is a consequence of the inherent infinite or semi-infinite extent of such profiles.

10. Several spatial frequency domain techniques for simulating the problem considered in this work were implemented, although testing was not completed. It is felt that a useful approach was identified.

11. A one-dimensional, time domain inverse scattering technique was simulated, including the effects of noisy data. The technique was demonstrated to be stable with respect to noise for typical ionspheric profiles. Errors in the reconstructed profile were less than or equal to the noise in the data, contrary to previous results. The technique permits the profile at altitudes above the maximum to be obtained using only bottomside vertical incidence sounder data. The approach appears readily applicable to the processing of data from existing sounders.

12. It has been shown that by choosing a short enough probing wavelength, the anisotropic properites of the ionosphere are negligable within the magneto-ionic theory approximations. This permits the use of scalar field measurements and scalar processing to obtain an accurate reconstruction of the electron density distribution.

13. It has been shown that in the short wavelength limit, the field reconstructed from a hologram is equal to i times the source term in the inverse scattering problem. Furthermore, for the case of the ionosphere within the framework

of the magneto-ionic theory, it has been shown that the magnitude of the field as a function of $\underline{x}$ obtained from a holographic reconstruction is directly proportional to the electron density as a function of $\underline{x}$.

7.2 RECOMMENDATIONS

The above conclusions each provide numerous possibilities for further research. The following recommendations highlight those areas deemed to be of most importance in the application of inverse scattering to the determination of the ionospheric electron density distribution.

1. Numerical evaluation of the exact, closed-form, analytic solution for the source should be studied, and the properties of the solution examined.
2. The deconvolution technique identified as most promising in Section 5.1 should be investigated, both analytically and numerically.
3. The simulation of the determination of the ionospheric density distribution should be developed, utilizing the spatial frequency domain techniques identified in this research to model the direct scattering.
4. The one-dimensional, time domain inverse technique should be studied, especially with regard to its properties in the presence of noise in the measurements. Application of the technique to data from existing sounders should be pursued.
5. An experimental observatory, using measurements such as were made in the Holographic Radio Camera demonstration experiment, processed using the inverse scattering techniques of this paper, should be established.

REFERENCES

1. H. G. Booker, "The Role of Acoustic Gravity Waves in the Generation of Spread F and Ionospheric Scintillation," J. Atmos. Ten. Phys., 41, 501-516, 1979.

2. K. Davies, Ionospheric Radio Propagation, Washington, U. S. Government Printing Office, 1966.

3. W. R. Stone, "Holographic Reconstruction is Usually a Poor Solution to the Inverse Scattering Problem: A Comparison Between the Bojarski Exact Inverse Scattering Theory and Holography as Applied to the Holographic Radio Camera," presented at the 1980 International Optical Computing Conference, April 8-11, 1980, Washington, DC; to appear in SPIE Proceedings, Vol. 231, 157-164, 1980.

4. W. R. Stone, "A Holographic Radio Camera Technique for the Three-Dimensional Reconstruction of Ionospheric Inhomogeneities," Journal of Atmospheric and Terrestrial Physics, Vol. 38, 583-592, 1976.

5. W. R. Stone, "The Concept, Design, and Operation of a Demonstration Holographic Radio Camera," Ph.D. dissertation, Applied Physics and Information Sciences, University of California, San Diego, 1978.

6. A. K. Jordan and S. Ahn, "Inverse Scattering Theory and Profile Reconstruction," N. R. L. Memorandum Report 3981, Naval Research Laboratory, April 17, 1979.

7. M. H. Reilly and A. K. Jordan, "The Applicability of An Inverse Method for Reconstruction of Electron Density Profiles," IEEE Trans. Ant. Prop., AP-29, 245-252, 1981.

8. N. N. Bojarski, "Inverse Scattering," Naval Air Systems Command, third quarterly report to Contract N00019-73-C-0312 (NASC-C2-Q3), October 1973.

9. N. N. Bojarski, "Inverse Scattering," Naval Air Systems Command, final report on Contract N00019-73-C-0312, February 1974.

10. N. N. Bojarski, "Exact Inverse Scattering," presented at the Annual Meeting of USNC/URSI, october 20-23, 1975, Boulder, Colorado.

11. N. Bleistein and N. N. Bojarski, "Recently Developed Formulations of the Inverse Problem in Acoustics and Electromagnetics," report MS-R-7501, (AD/A-003 588) Department of Mathematics, Denver Research Institute, University of Denver, Colorado, 1974.

12. J. A. Stratton, Electromagnetic Theory, New York, McGraw-Hill Book Company, 1941.

13. B. S. Tanenbaum, Plasma Physics, New York, McGraw-Hill Book Company, 1967.

14. K. G. Budden, Radio Waves in the Ionosphere, Cambridge, University Press, 1961.

15. N. Bleistein and J. Cohen, "Nonuniqueness in the Inverse Source Problem in Acoustics and Electromagnetics," Journal of Mathematical Physics, 18, 194-201, 1977.

16. W. R. Stone, "A Uniqueness Proof for the Bojarski Exact Inverse Scattering Theory, and Its Consequences for the Holographic Radio Camera," presented at the URSI National Radio Science Meeting, Boulder, Colorado, January 9-13, 1978.

17. J. A. Kong, Theory of Electromagnetic Waves, New York, John Wiley & Sons, 1975.

18. A. J. Devaney and E. Wolf, "Radiating and Nonradiating Classical Current Distributions and the Fields They Generate," Phys. Rev. D, 8, 1044-47, 1973.

19. A. J. Devaney, "Nonuniqueness in the Inverse Scattering Problem," J. Math. Phys., 19, 1526-31, 1978.

20. W. R. Stone, "Nonradiating Sources of Compact Support Do Not Exist: Uniqueness of the Solution to the Inverse Scattering Problem," J. Opt. Soc. Am., 70, 1606, 1980.

21. R. Bracewell, The Fourier Transform and Its Applications, New York, McGraw-Hill Book Company, 1965.

22. N. N. Bojarski, private communication, September 1981.

23. R. P. Porter and A. J. Devaney, "Holography and the Inverse Source Problem," submitted to J. Opt. Soc. Am., 1981.

24. N. N. Bojarski, "Inverse Scattering Inverse Source Theory," Office of Naval Research, Contract N00014-76-C-0082, November 1980.

25. N. N. Bojarski, "Inverse Scattering Inverse Source Theory," J. Math. Phys., 22. 1647-50, 1981.

26. W. R. Stone, "How to Get off the Fourier Domain ('Ewald') Sphere in the Inverse Scattering Problem," presented at the National Radio Science Meeting of USNC/URSI, Boulder, Co, January 12-16, 1981.

27. R. F. Harrington, Time Harmonic Electromagnetic Fields, New York, McGraw-Hill Book Company, 1961, Equation 4-124.

28. G. C. Sherman, "Application of the Convolution Theorem to Rayleigh's Integral Formulas," J. Opt. Soc. Am., 57, 546-547, 1967.

29. R. M. Gray, "Toeplitz and Circulant Matrices: II," Stanford University Information Systems Laboratory, Technical Report No. 6504-1 (SEL-77-011), April 1977.

30. J. H. Wilkinson, "The Solution of Ill-Conditioned Linear Equations," in A. Ralston and H. S. Wilf (eds.) Mathematical Methods for Digital Computers, New York, John Wiley & Sons.

31. S. Zohar, "Toeplitz Matrix Inversion: The Algorithm of W. F. Trench," J. A. C. M., 16, 592-601, 1969.

32. E. H. Bareiss, "Numerical Solution of Linear Equations with Toeplitz and Vector Teoplitz Matrices," Numer. Math., 13, 404-424, 1969.

33. D. H. Preis, "The Toeplitz Matrix: Its Occurrence in Antenna Problems and a Rapid Inversion Algorithm," IEEE Trans. Ant. Prop., AP-20, 204-6, 1972.

34. D. H. Sinnott, "Matrix Analysis of Linear Antenna Arrays of Equally Spaced Elements," Department of Supply, Australian Defence Scientific Service, Weapons Research Establishment, Salisbury, South Australia, WRE-Technical Note 622(AP), May, 1972.

35. G. A. Watson, "An Algorithm for the Inversion of Block Matices of Toeplitz Form," J. A. C. M., 20, 409-415, 1973.

36. H. Akaike, "Block Toeplitz Matrix Inversion," SIAM J. Appl. Math., 24, 234-41, 1973.

37. D. H. Sinnott, "An Improved Algorithm for Matrix Analysis of Linear Antenna Arrays," Department of Supply, Australian Defence Scientific Service, Weapons Research Establishment, Salisbury, South Australia, WRE-Technical Memorandum-1066(AP), January, 1974.

38. D. C. Farden, "Solution of a Toeplitz Set of Linear Equations," IEEE Trans. Ant. Prop., AP-24, 906-7, 1976.

39. T. Kailath, A. Vierra, and M. Morf, "Inverses of Toeplitz Operators, Innovations, and Orthogonal Polynomials," SIAM Review, 20, 106-119, 1978.

40. J. R. Jain, "An Efficient Algorithm for a Large Toeplitz Set of Linear Equations," IEEE Trans. Acous. Speech Sig. Process., ASSP-27, 612-615, 1979.

41. S. Zohar, "Fortran Subroutines for the Solution of Toeplitz Sets of Linear Equations," IEEE Trans. Acous. Speech Sig. Process., ASSP-27, 656-58, 1979; correction in ASSP-28, 601, 1980.

42. D. H. Sinnott, "An Algorithm for Solution to a System of Linear Equations with Coefficient Matrix of General Block - Toeplitz Form," unpublished manuscript/private communications, May, 1981.

43. M. Morf, "Doubling Algorithms for Toeplitz and Related Equations," in Proceedings of International Conference on Acoustics, Speech, and Signal Processing, Denver, Colorado, 954-959, April 9-11, 1980.

44. R. P. Brent, F. G. Gustavson, and D. Y. Y. Yun, "Fast Solution of Toeplitz Systems of Equations and Computation of Padé Approximants," J. Algorithms, 1, 259-95, 1980.

45. F. G. Gustavson and D. Y. Y. Yun, "Fast Algorithms for Rational Hermite Approximation and Solution of Toeplitz Systems," IEEE Trans. Cir. Sys., CAS-26, 750-54, 1979.

46. R. R. Bitmead and B. D. O. Anderson, "Asymptotically Fast Solution of Toeplitz and Related Systems of Linear Equations," Linear Algebra and Its Applications, 34, 103-116, 1980.

47. S. Wood, private communications, April - September 1981.

48. H. C. Andrews and B. R. Hunt, Digital Image Restoration, Englewood Cliffs (NJ), Prentice-Hall Inc., 1977.

49. R. C. Gonzalez and P. Wintz, Digital Image Processing, Reading (MA), Addison-Wesley Publishing Co., 1977.

50. R. M. Gray, "On the Asymptotic Eigenvalue Distribution of Toeplitz Matrices," IEEE Trans. Info. Theory, IT-18, 725-30, 1972.

51. M. P. Ekstrom, "An Iterative - Improvement Approach to the Numerical Solution of Vector Toeplitz Systems," IEEE Trans. Computers, C-23, 320-325, 1974.

52. W. R. Stone, "Numerical Studies of the Effects of Noise and Spatial Bandlimiting on Source Reconstructions Obtained using the Bojarski Exact Inverse Scattering Theory," presented at the URSI spring meeting, College Park, Maryland, May 15-19, 1978.

53. W. R. Stone, "The Inverse Scattering Problem Has a Numerically Well-Posed Solution," presented at the URSI National Radio Science Meeting, Boulder, Colorado, January 12-16, 1981.

54. B. R. Hunt, "The Application of Constrained Least Squares Estimation to Image Restoration by Digital Computers," IEEE Trans. Computers, C-22, 805-812, 1973.

55. P. S. Epstein, "Reflection of Waves in an Inhomogeneous Absorbing Medium," Proc. Nat. Acad. Sci., 16, 627-637, 1930.

56. C. J. Mullin, "Solution of the Wave Equation Near an Extremum of the Potential," Phys. Rev., 92 (Second Ser.), 1323-24, 1953.

57. R. Yamada, "On the Radio Wave Propagation in a Stratified Atmosphere," J. Phys. Soc. Japan, 10, 71-77, 1955.

58. I. L. Gazarian, "The Problem of Waveguide Propagation of Sound in Inhomogeneous Media," Soviet Phys. Acoustics, 2, 134-138, 1956.

59. I. L. Garzarian, "Waveduct Propagation of Sound for One Particular Class of Laminarly - Inhomogeneous Media," Soviet Phys. Acoustics, 3, 135-149, 1957.

60. A. T. de Hoop, "A Note on the Propagation of Waves in a Continuously Layered Medium," Appl. Sci. Rev., 12 (Sec B), 74-80, 1964.

61. J. R. Catchpoole, "On Certain Exact Wave Functions for Electromagnetic Fields in Planar Stratified Media," J. Atmos. Terr. Phys., 26, 1127-29, 1964.

62. H. Blok, "The Electromagnetic Field Generated by a Dipole in an Epstein Medium," in J. Brown (ed.), Electromagnetic Wave Theory, Part 1 (URSI Symposium on Electromagnetic Wave Theory, Technilogical University of Delft, September 1965), Oxford, Pergamon Press, 135-146, 1965.

63. R. L. Deavenport, "A Normal Mode Theory of an Underwater Acoustic Duct by Means of Green's Function," Radio Science, 1, 709-24, 1966.

64. H. P. Bucker and H. E. Morris, "Epstein Normal - Mode Model of a Surface Duct," J. Acoust. Soc. Am., 41, 1475-78, 1967.

65. J. Heading, "Investigations Into a New Stratified Hyperbolic Profile, Proc. Camb. Phil. Soc., 63, 439-50, 1967.

66. M. A. Pedersen and D. W. White, "Ray Theory of the General Epstein Profile," J. Acous. Soc. Am., 44, 765-86, 1968.

67. J. Heading, "Polarization of Obliquely Reflected Waves From an Isotropic Plane - Stratified Plasma, " Radio Science, 4, 441-47, 1969.

68. J. R. Waite, "Oblique Reflection of a Plane Impulsive Electromagnetic Wave from a Plasma Half-Space," Phys. Fluid, 12 (Part 2), 1521-22, 1969.

69. K. F. Casey, "Application of Hill's Functions to Problems of Propagation in Stratified Media," IEEE Trans. Ant. Prop., AP-20, 368-374, 1972.

70. L. M. Brekhovskikh, "Waves in Layered Media," second edition, New York, Academic Press, 1980.

71. J. R. Wait, Electromagnetic Waves in Stratified Media, Oxford, Pergamon Press, 1970.

72. N. N. Bojarski, "K-Space Formulation of the Electromagnetic Scattering Problem," Air Force Avionics Laboratory Technical Report AFAL-TR-72-271, September 1972.

73. C. Kruger, "K-Space Formulation of the Two-Dimensional Electromagnetic Scattering Problem," Ph.D. dissertation in Electrical Engineering, Ohio State University, 1972.

74. R. Kastner and R. Mittra, "A Spectral-Iteration Technique for Analyzing Scattering From Arbitary Bodies," presented at IEEE Antennas and Propagation Society International Symposium, Los Angeles, June 16-19, 1981.

75. R. Mittra, "Plane-Wave Spectral Techniques," presented at the XXth General Assembly of URSI, Washington, D.C., August 10-19, 1981.

76. R. Mittra, private communication, September 1981.

77. N. N. Bojarski, "Direct and Inverse Scattering in Causal Space," Wave Motion, 2, 115-124, 1980.

78. W. R. Stone, "Numerical Considerations in the Application of the Exact Inverse Scattering Theory," presented at the 17th Annual Meeting of the Society of Engineering Science, Atlanta, Georgia, December 15-17, 1980.

79. R. D. Mager and N. Bleistein, "An Examination of the Limited Aperture Problem of Physical Optics Inverse Scattering," IEEE Trans. Ant. Prop., AP-26, 695-699, 1978.

80. W. R. Stone, "The Resolution of an Aperture for Coherent Imaging," J. Opt. Soc. Am., 68, 1404, 1978.

81. W. M. Lewis, "Physical Optics Inverse Scattering," IEEE Trans. Ant. Prop., AP-17, 308-314, 1969.

82. J. W. Goodman, Introduction to Fourier Optics, San Francisco, McGraw-Hill, 1968.

83. R. J. Collier, C. B. Burckhardt, and L. H. Lin, Optical Holography, New York, Academic Press, 1971.

84. H. G. Booker, J. A. Ratcliffe, and D. H. Shinn, Phil. Trans. Royal Society, A242, 579-607, 1950.

85. C. L. Rufenach, Radio Science, 10, 155-156, 1975.

86. E. N. Bramley, J. Atmos. Terr. Phys., 39, 367-373, 1977.

87. H. G. Booker, "Acoustic Gravity Waves, Traveling Ionospheric Disturbances, Spread F and Ionospheric Scintillation," presented at the 60th Anniversary of the International Union of Radio Science, Brussels, Belgium, September 1979; and at the National Radio Science Meeting, Boulder, Colorado, November 1979.

88. H. G. Booker, "The Role of Acoustic Gravity Waves in the Generation of Spread F and Ionospheric Scintillation," J. Atmos. Terr. Phys., 41, 501-516, 1979.


FILMED
4-8